METHODOLOGIES AND APPLICATION

Design of new fractional order PI–fractional order PD cascade controller through dragonfly search algorithm for advanced load frequency control of power systems

Emre Çelik[1] 🔘

Abstract

Owing to integrating the dense range of distinct electric power sources, high volume of power generation units, abrupt and continuous changes in load demand, and rising utilization of power electronics, the electric power system (EPS) is striving for high-performance control schemes to counterwork the concerns depicted above. Additionally, it is highly creditable to have the controller structure as simple as possible from a viewpoint of practical implementation. Thus, this paper describes a virgin application of fractional order proportional integral–fractional order proportional derivative (FOPI–FOPD) cascade controller for load frequency control (LFC) of electric power generating systems. The proposed controller includes fractional order PI and fractional order PD controllers connected in cascade wherein orders of integrator (λ) and differentiator (μ) may be fractional. The gains and fractional order parameters of the controller are concurrently tuned using recently proposed dragonfly search algorithm (DSA) by minimizing the integral time absolute error (ITAE) of frequency and tie-line power deviations. DSA is the mathematical model and computer simulation of static and dynamic swarming behaviors of dragonflies in nature, and its implementation in LFC studies is very rare, unveiling additional research gap to be bridged. Performance of the advocated approach is first explored on popular two-area thermal PS with/without governor dead band (GDB) nonlinearity and then on three-area hydrothermal PS with suitable generation rate constraints. To highlight the prominence and universality of our proposal, the work is extended to single-/multi-area multi-source EPSs. Several comparisons with DSA optimized FOPID controller and the relevant recent works for each test system indicate the contribution of proposed DSA optimized FOPI–FOPD cascade controller in alleviating settling time/undershoot/overshoot of frequency and tie-line power oscillations.

Keywords Load frequency control · Governor dead band · Generation rate constraint · Fractional order PI–fractional order PD (FOPI–FOPD) cascade controller · Dragonfly search algorithm · Optimization

1 Introduction

The essential function of an electric power system (EPS) is to deliver electrical energy to its consumers economically and efficiently. Herein, the economical aspect of electricity delivery covers the problem of optimal power flow (OPF), which is one of the most crucial issues in EPS operation and modern energy management system and it has been among the widely studied subjects by researchers (Naderi et al. 2019; Mandal and Roy 2014). What it is meant by "efficiently" dictates the quality of electric power energy which requires to balance generated, transmitted and distributed active powers. Any undesirable mismatch between generation and load demand resulting from unpredictable internal/external disturbances and/or load changes causes deviation of system operational frequency and interchange tie-line power flow from their scheduled limits. This brings out an aspiration for designing an accurate, efficient and fast control mechanism in PS modeling called load frequency control (LFC) to keep system performance measures, i.e. area frequency and interchange tie-line power, at their scheduled values. Indeed, LFC is one of the most profitable ancillary services to be well handled for the

---

✉ Emre Çelik
emrecelik@duzce.edu.tr

1   Department of Electrical and Electronics Engineering,
    Engineering Faculty, Düzce University, Düzce, Turkey

smooth and secure operation of EPS (Singh et al. 2017). It is aiming to diminish quickly transient deviations of area frequency and interchange tie-line power flow between the nearby control areas and to maintain their steady state errors at zero. Such mission in our today's world where several types of electricity generating units contribute to total electricity generation is becoming much more crucial for offering eligible and reliable electrical power with high quality to the use by the consumer. A summarize of the main tasks of LFC is given as stepdown (Singh et al. 2017; Guha et al. 2016, 2017).

1. The system in the wake of abrupt load disruption and any of disturbances must be kept under control.
2. Undershoot, overshoot and settling time of frequency and tie-line power deviations should be reduced so as to raise the system stability margin.
3. Following a step load perturbation (SLP), area control error (ACE) must be eliminated as much as possible.
4. Each area should accommodate its own load at steady state.
5. Areas in need of power can collaborate with each other at transient state.

In view of the above, researchers worldwide are notably endeavoring to introduce betterment in LFC of EPSs. Since the performance of LFC system is shown to greatly link with the controller structure and the tuning algorithm exploited to optimize the controller gains, this betterment may appear in three ways. A critical literature review on this topic points out that in some works, new high-performance optimization algorithms are employed to optimize the gains of classical techniques (i.e. PI/PID) in order to enhance their capabilities. The second portion of literature survey includes studies where a new controller scheme is proposed and its parameters are tuned by a base search algorithm to avoid misleading control performance owing to improper parameter adjustment. In the last scenario, researchers take benefits of the first two solutions in that a new controller structure is presented and its parameters are adjusted through using a powerful optimizer newly proposed which favorably bestows superior search performance comparing to its predecessors. Among the three approaches, the last one based on an original control scheme and new search algorithm is always appreciated to find a LFC mechanism better than the existing ones in the literature.

Our literature inspection points out that a great number of control approaches in conjunction with proper optimization techniques are available to handle LFC problem of interconnected EPS. It is shown that researches on LFC that concentrate on the design of classical integer controllers are extensive. Some of them are quasi-oppositional grey wolf optimization algorithm (QOGWO)-based PID

(Guha et al. 2016), quasi-oppositional symbiotic organisms search (QOSOS) algorithm-based PI/PID (Guha et al. 2017), bacterial foraging optimization algorithm (BFOA)-based PI controller (Ali and Abd-Elazim 2011), artificial bee colony (ABC) technique-based PI/PID (Gozde et al. 2012), hybrid BFOA and particle swarm optimization (PSO) (hBFOA-PSO) algorithm-based PI (Panda et al. 2013), differential evolution (DE) algorithm-based I/PI/PID (Mohanty et al. 2014), backtracking search algorithm (BSA)-based PI/PID (Guha et al. 2018), quasi-oppositional harmony search algorithm (QOHS)-based PID (Shiva et al. 2015), differential search algorithm (DSA)-based PID (Guha et al. 2017), hybrid firefly algorithm-pattern search (hFA-PS) technique-based PI/PID (Sahu et al. 2015), grey wolf optimization (GWO)-based PI/PID (Guha et al. 2016), and DE-based PID (Hota and Mohanty 2016). Also, modified versions of PID control schemes such as bat algorithm-based dual mode PI (Sathya and Ansari 2015), hybrid stochastic fractal search and local unimodal sampling (hSFS-LUS)-based multistage PID (Sivalingam et al. 2017), GWO technique-based cascade PI–PD controller (Padhy et al. 2017), flower pollination algorithm (FPA)-based PI–PD cascade controller (Dash et al. 2016), and different optimization techniques-based two-degree-of-freedom (2DOF) controllers (Sahu et al. 2013, 2016; Dash et al. 2014; Patel et al. 2019) have been proposed. To deal with the nonlinear behavior of LFC problem and guarantee, the system stability under stochastic load pattern and disrupting inputs, alternative control approaches based on sliding modes (Vrdoljak et al. 2010), artificial neural network approach (Saikia et al. 2011), fuzzy logic theory (Sahu et al. 2015, 2016; Nayak et al. 2018; Arya and Kumar 2017), adaptive neuro fuzzy inference system (ANFIS) (Khuntia and Panda 2012) and fractional order calculus (Sondhi and Hote 2014; Arya 2019a, b; c) have been also focused. Clearly, these controllers are computationally more expensive and difficult to design than classical techniques, but they eliminate the restrictions caused by their traditional counterparts and performance increases achieved by them are affirmed significant.

What makes a control strategy essential is that it should have good capability of tackling parameter uncertainties with good disturbance rejection while yielding the desirable dynamic performance as much as possible. Also, the design task of controller applied should not be so complicated for having a practical solution for engineering commissioning. These metrics have always remained major issues and continuous efforts are paid to generate new control schemes which are able to deal with the above-stated concerns. A recent development in this way is the formulation of non-integer or fractional order controllers which does not necessarily suggest the use of integer (i.e. 1.0), but any real numbers for orders of integrator and

differentiator. It is unveiled from the literature that the fractional order (FO) controller is known to exhibit better dynamic response with an excellent robustness to parameter uncertainty and external disturbances. It also yields better stability in presence of nonlinear systems (Sondhi and Hote 2014). All these properties make the FO control popular and desirable strategy in several areas such as power electronics, robotics and process control (Jezierski and Ostalczyk 2009; Saha 2010; Jesus et al. 2010). Moreover, researches taking the advantages of FO theory in the field have been emerged densely in the literature such as fractional order PID (FOPID) (Sondhi and Hote 2014), gases Brownian motion optimizer (GBMO) (Zamani et al. 2016), hybridized gravitational search algorithm (DOGSA) (Dahiya et al. 2015) and big bang-big crunch (BBBC) (Kumar et al. 2016)-based FOPID, BFOA-based FO fuzzy PID (FOFPID) (Arya and Kumar 2017; Arya 2019d), imperialist competitive algorithm (ICA)-based fuzzy FO integral derivative (FFOID) (Arya 2019a) and cascaded fuzzy FOPI-FOPID (CFFOPI-FOPID) (Arya 2019b) controllers. Nonetheless, collective functioning of FOPI and FOPD in a cascaded connection, i.e. FOPI–FOPD, has not been yet evaluated as supplementary controller in LFC of EPSs. As such, encouraged by such a research gap, this paper offers a new FOPI–FOPD cascade controller and investigates its application to the problem of LFC. To procure the best set of FOPI–FOPD cascade controller parameters for avoiding improper gain adjustment, dragonfly search algorithm (DSA) is utilized as the powerful optimizer whose application to the studied problem is very rare, and thus needs further investigation. This constitutes the secondary contribution of this work.

DSA is a new nature-inspired algorithm, recently proposed by (Seyedali 2016), which mitigates the identified characteristics of the individual and social intelligence of fancy insects called dragonflies (Odonata). Two essential milestones exist in a dragonfly's lifecycle namely nymph and adult. The greater portion of dragonflies' lifespan is spent in nymph and they experience metamorphism thereafter to become adult. Swarming behavior of dragonflies are found interesting and rare in that they swarm for only two aims: hunting and migration. Hunting is called static (feeding) swarm and migration is called dynamic (migratory) swarm which can be considered as the foundation blocks of DSA. In static swarm, dragonflies are divided into small groups and fly within a small area to hunt other flying preys. The salient properties of this sort of swarm are local movements and sudden changes in the flying path. For dynamic swarms, a great number of dragonflies are assumed and they let the swarm migrate in one direction over long distances. The efficacy and competence of DSA is judged for several optimization problems like function optimization and designing a real propeller for submarines (Seyedali 2016), optimal load

frequency regulation of micro-grid (Venkatesh and Sudheer 2017), designing a combined fuzzy PID controller for solving LFC problem (Nour et al. 2018), etc., by comparing the results obtained to the prior results in the relevant literature. Though there have been numerous LFC studies with various optimization techniques, few of them tackle the LFC problem employing the DSA approach (Venkatesh and Sudheer 2017; Nour et al. 2018). As a result, the participation of DSA in the concerned problem is a research avenue and worthy to be studied.

In view of the above, a new fractional order proportional integral-fractional order proportional derivative (FOPI–FOPD) cascade controller is constructed to ameliorate LFC performance of interconnected multi-area power units. To get the performance of this controller as nearer to optimality as possible, DSA is employed to tune the controller parameters like proportional gains (K_p, K_{p1}), integral gains (K_i, K_{i1}), order of integrator (λ) and order of differentiator (μ) by minimizing the value of integral time absolute error (ITAE) criterion. Widely employed two-area thermal EPS with/without governor dead band (GDB) nonlinearity, three-area hydrothermal EPS with suitable generation rate constraints (GRCs) and also single-/multi-area multi-source EPSs are considered to establish the expected performance of advocated approach. Several results obtained by simulating the networks are presented in comparison with DSA tuned FOPID controller and the available results reported earlier to betoken the reputation of the method. It is divulged that DSA is a powerful means to search for the controller parameters in the studied control application and DSA tuned FOPI–FOPD cascade controller is able to provide valuable contributions to the relevant field.

The rest of the paper is arranged as follows. Section 2 presents the transfer function models of various EPSs tested. A brief overview of fractional calculus is given in Sect. 3. This section also details the structure of proposed FOPI–FOPD cascade controller and its formulation from the optimization point of view. DSA is studied in Sect. 4. To show and verify the contribution of the advocated approach, a comprehensive comparative study on the respective test cases is conducted with several reported methodologies in Sect. 5. Finally, some concluding notes and useful suggestions for future search directions are provided in Sect. 6.

2 Systems investigated

2.1 Classical two-area interconnected thermal power system

Investigations have been performed first on two-area interconnected thermal EPS with and without governor

dead band (GDB) nonlinearity. The transfer function models of these systems that are widely employed in the literature for benchmarking LFC solution (Ali and Abd-Elazim 2011; Gozde et al. 2012; Panda et al. 2013; Guha et al. 2017, 2018; Shiva et al. 2015) are sketched in Fig. 1. These systems will be referred to as test system-1 and test system-2, respectively, in this paper. Each area of the EPS is outfitted with one non-reheat turbine and one speed governor-based thermal generating unit.

Each control area has three inputs and two outputs. The inputs are the controller output ΔP_{ref}, load disturbance ΔP_D and tie-line power error ΔP_{tie}. The outputs are the generator frequency error Δf and area control error (ACE) represented by Eq. 1.

$$ACE = -B\Delta f \pm \Delta P_{tie} \tag{1}$$

where B is the frequency bias parameter.

Non-reheat turbine is modeled by the following transfer function with T_t being the time constant of steam turbine.

$$G_t(s) = \frac{\Delta P_t}{\Delta P_g} = \frac{1}{sT_t + 1} \tag{2}$$

The model of a speed governor is first considered linear and represented by Eq. 3 where T_g is the time constant of speed governor.
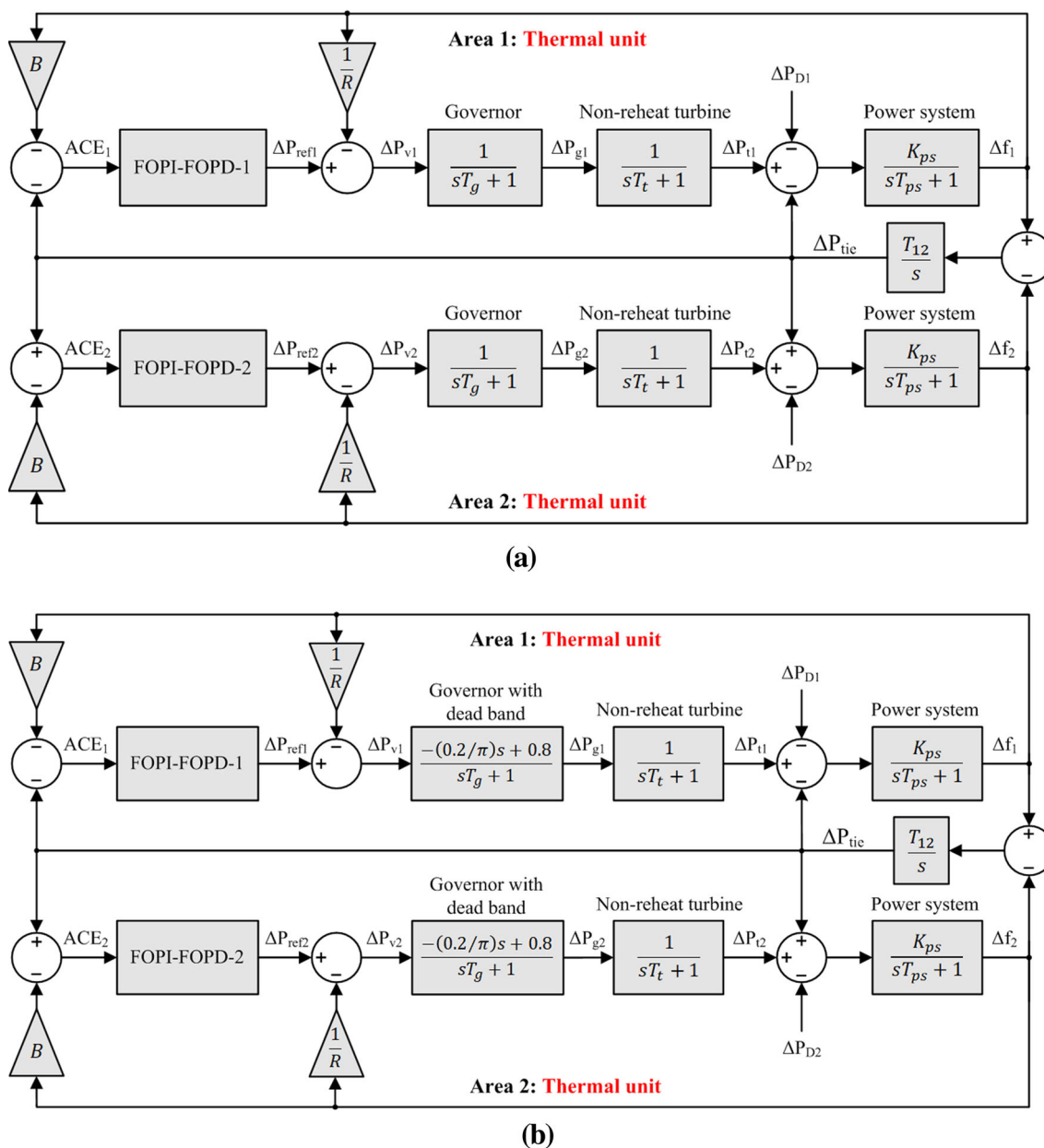

(a)

(b)

Fig. 1 Transfer function model of two-area interconnected non-reheat thermal EPS **a** without GDB nonlinearity **b** with GDB nonlinearity

$$G_g(s) = \frac{\Delta P_g}{\Delta P_v} = \frac{1}{sT_g + 1} \qquad (3)$$

To get a more realistic insight into the LFC issue, it is required some nonlinearities emerging in a real system be included in EPS modeling. In this direction, a nonlinearity source called governor dead band (GDB) is considered in this paper to investigate its influence on the EPS dynamics. GDB makes the system behave oscillatory and described as the total amount of a maintained speed variation within which valve position does not change. A describing function-based technique is utilized to integrate GDB nonlinearity and the transfer function of governor with dead band is given by

$$G_g(s) = \frac{\Delta P_g}{\Delta P_v} = \frac{-(0.2/\pi)s + 0.8}{sT_g + 1} \qquad (4)$$

The input of speed governor is ΔP_v which is calculated by subtracting $\frac{1}{R}\Delta f$ from ΔP_{ref} as in Eq. 5 where R is a parameter for speed regulation of speed governor and ΔP_{ref} is reference power command to be generated.

$$\Delta P_v = \Delta P_{ref} - \frac{1}{R}\Delta f \qquad (5)$$

The pair of generator (rotating mass) and load is represented by a gain K_{ps} and time constant T_{ps} given by

$$G_p(s) = \frac{K_{ps}}{sT_{ps} + 1} \qquad (6)$$

Eventually, frequency error or frequency deviation is obtained from the output of the system as

$$\Delta f(s) = G_p(s)[\Delta P_t(s) - \Delta P_D(s) - \Delta P_{tie}] \qquad (7)$$

ΔP_{tie} is the deviation of tie-line power flowing in-between neighboring control areas at transient states and computed by

$$\Delta P_{tie} = \frac{T_{12}}{s}[\Delta f_1 - \Delta f_2] \qquad (8)$$

where T_{12} is the synchronizing time constant of tie-line.

In Fig. 1, the two areas are considered identical and so are the controllers in both areas such that FOPI-FOPD-1 $\equiv$ FOPI-FOPD-2.

2.2 Three-area hydrothermal power system

A three-area hydrothermal EPS is designed and employed to see the ability of the proposed approach in dealing with interconnected multi-area EPS. This system, named as test system-3, has three generating units where areas 1 and 2 are thermal based on single-stage reheat turbines, whereas area 3 is a hydro one driven by an electric governor as depicted in Fig. 2. In such a system, because all the areas are fully connected with each other, tie-line power transfer

between two neighboring areas does not necessarily flow directly through the tie lines connecting the associated areas, but may occur over parallel lines via other areas. Since the thermal areas are of the same type, both controllers in these areas are decided identical and different from that in the hydro area. This way, we have reduced the number of controllers in need of being tuned concurrently from three to two for simplification.

It is known that the power generation in an EPS cannot change at an infinite rate, but at a certain rate depending on the physical limits of system mechanics and dynamics. To limit the rate of generation, a significant constraint called generation rate constraint (GRC) is considered for all the areas in Fig. 2. The related works in the literature suggest that the standard value of GRC for a thermal area is 3%/min. So, GRC for the ith thermal system is

$$|\Delta P_{Gi}(s)| \leq 0.0005 \quad \text{p.u MW/s}$$

Two saturation blocks restricted by ± 0.0005 are added into the thermal units to evade from excessive generation. Likewise, for the hydro area, different generation amounts, 360%/min for lowering generation and 270%/min for raising generation, are considered. Thus,

$$|\Delta P_G(s)| \leq 0.06 \quad \text{p.u MW/s} \Rightarrow \text{ for lowering}$$
$$|\Delta P_G(s)| \leq 0.045 \quad \text{p.u MW/s} \Rightarrow \text{ for raising}$$

This has been taken into account in the system model by including a saturation block limited by -0.06 and 0.045 in the hydro turbine.

2.3 Extension to multi-source power system

After the initial investigations on linear/nonlinear two-area non-reheat thermal and three-area hydrothermal EPSs, the study is extended to more practical multi-source EPS to further qualify the performance of DSA tuned FOPI–FOPD cascade controller. A single-area and two-area EPS having three generating units in each area are considered in this section. In such systems, collective performance of all generators of different types is interested.

a. Multi-source single-area power system

Transfer function model of a multi-source single-area power plant is illustrated in Fig. 3. The plant, designated as test system-4, has three individually controlled generating units of thermal with reheat turbine, hydro and gas units. Each generating unit has its own regulation parameter and participation factor, which decide the contribution of the respective unit to the total generation. The summation of participation factors of all participating generators should be equal to unity in a control area. In Fig. 3, R is the regulation parameter, U_T, U_H and U_G are controller outputs of thermal, hydro and gas units, respectively, K_T, K_H and
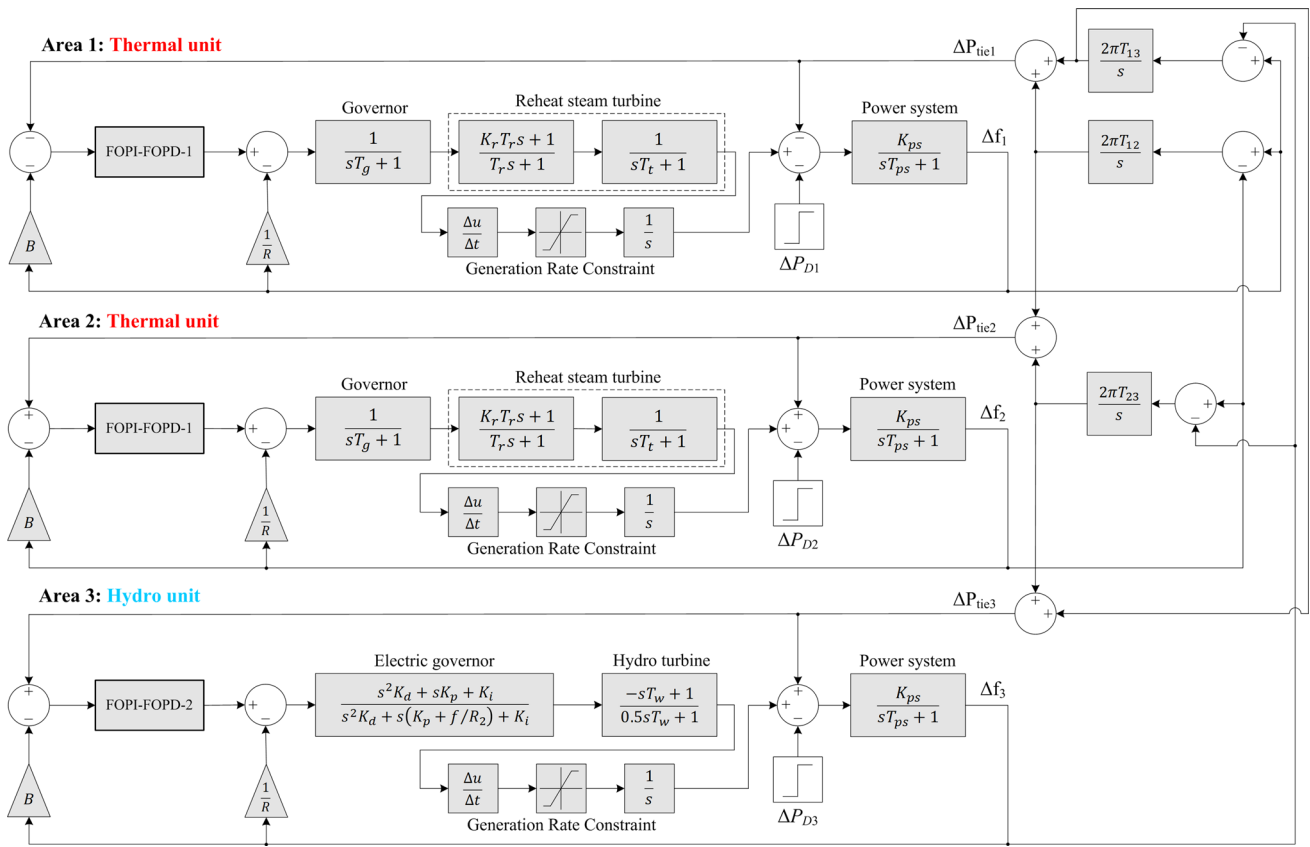
Fig. 2 Transfer function model of three-area interconnected hydrothermal EPS
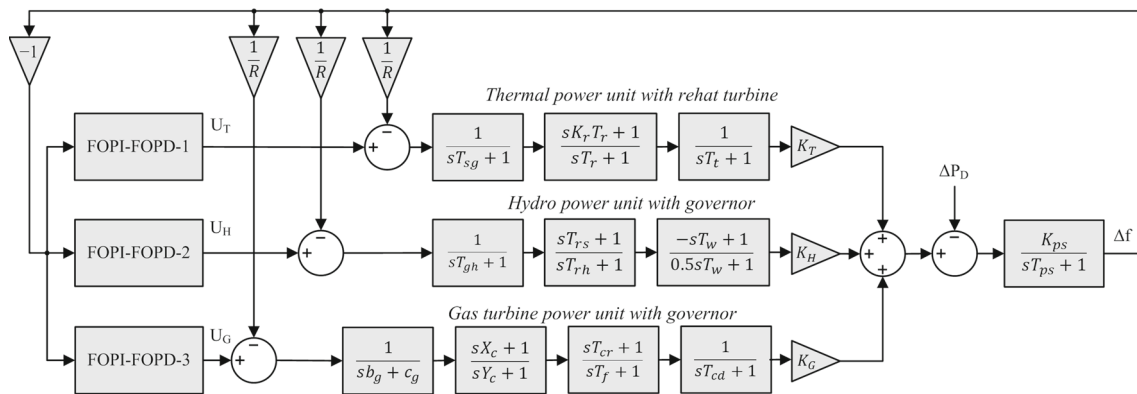

Fig. 3 Transfer function model of multi-source single-area EPS

K_G are participating factors of thermal, hydro and gas units, respectively, T_{sg} is speed governor time constant of thermal unit, K_r and T_r are reheat gain and reheat time constant, respectively, T_t is steam turbine time constant, T_{gh} is main servo time constant of hydro turbine speed governor, T_{rs} and T_{rh} are reset time and transient droop time constant of hydro turbine speed governor, respectively, and T_w is given as nominal starting time of water in penstock. As for gas turbine power unit, c_g is gas turbine valve positioner, b_g is gas turbine constant of valve positioner, X_c and Y_c are lead and lag time constant of gas turbine speed governor, respectively, T_{cr}, T_f and T_{cd} are combustion reaction time delay, fuel time constant and compressor discharge volume-time constant of gas turbine, respectively. K_{ps} and T_{ps} are gain and time constant of EPS, respectively, Δf is frequency deviation and ΔP_D is incremental change in load.

b. Two-area multi-source power system

The efficacy of the proposed control scheme is finally examined on test system-5 that considers a two-area six-unit multi-source EPS as shown in Fig. 4. In fact, each area of this plant is familiar with multi-source single-area system in Fig. 3 and the only difference between two power plants is the AC tie line that interconnects two control areas for load sharing purpose during transient state. Since the two areas are assumed identical, we consider the three controllers in both areas to be identical also. This eliminates the necessity for effective tuning of each of six controllers for each generating unit, which is both costly from the optimization viewpoint and impractical in real-time implementation.

3 Controller synthesis

3.1 A mini overview of fractional calculus

Control system engineering has witnessed noticeable increase in exploiting fractional order (FO) controllers owing to their properties of short response time, good stability under varying circumstances and excellent robustness to external disturbances. The idea underlying the use of FO dates back the study of Oustaloup et al. (2000). Later on, Podlubny introduced a general scheme of standard PID controller designated as FOPID or $PI^\lambda D^\mu$ controller (Podlubny 1999). Then, many research papers taking benefits of FOPID controller have appeared in several application areas such as automatic voltage regulator (Zeng et al. 2015), twin rotor helicopter (Azarmi et al. 2015), trajectory control (Mousavi and Alfi 2015), solid-core magnetic bearing system (Zhong and Li 2015) as well as load frequency control of diverse EPSs (Khuntia and Panda 2012; Kumar et al. 2016; Arya and Kumar 2017; Arya 2019d; Ismayil et al. 2014; Nithilasaravanan et al. 2019; Pan and Das 2015). The concept of FO controller corresponds to differential equations through fractional calculus (FC), which is the generalization of the ordinary calculus making use of the richness provided by the non-integer order of Laplace variable s. That said, it is an extension of $d^n y(t)/dt^n$ concept with n being an integer number to the concept $d^\alpha y(t)/dt^\alpha$ with α being a non-integer number. As the result of this generalization, another basic operator, named fractional integro-differential operator $_aD_t^\alpha$, has been evolved as
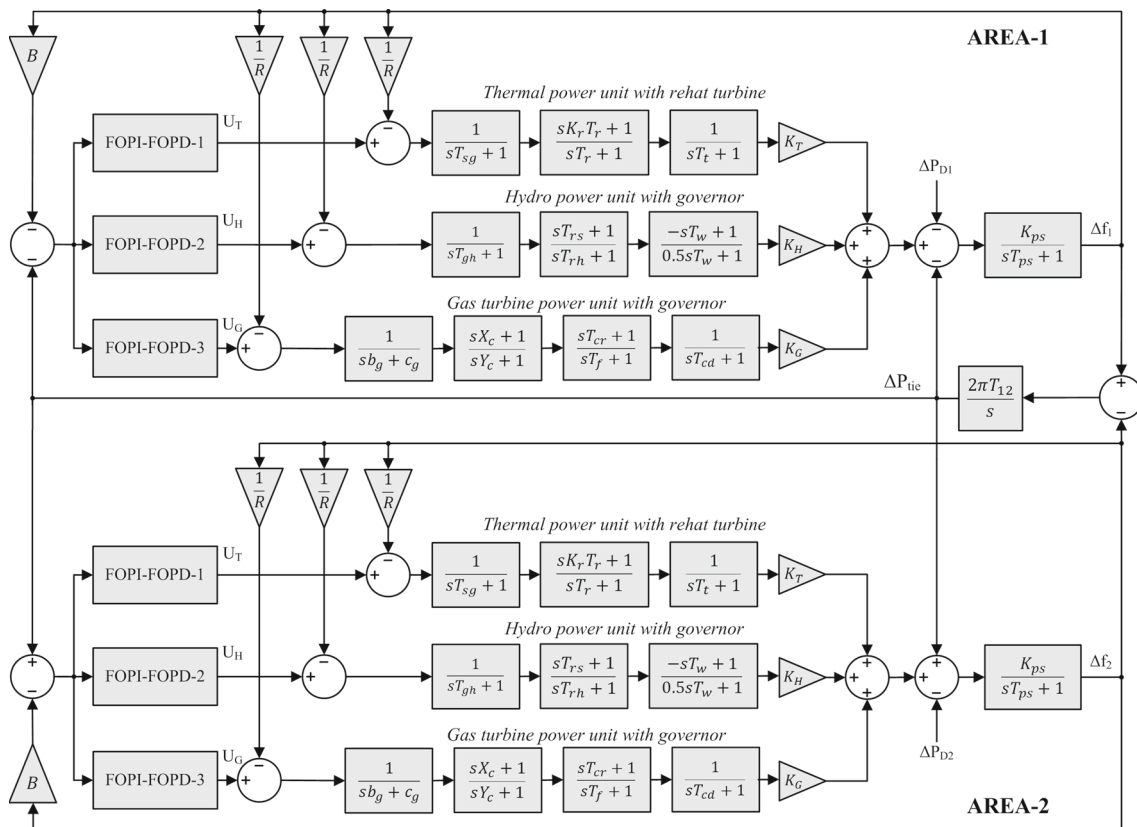

Fig. 4 Transfer function model of two-area multi-source EPS

$$_aD_t^\alpha = \begin{cases} \dfrac{\mathrm{d}^\alpha}{\mathrm{d}t^\alpha} & R(\alpha) > 0 \\ 1 & R(\alpha) = 0 \\ \displaystyle\int_a^t (\mathrm{d}\tau)^{-\alpha} & R(\alpha) < 0 \end{cases} \qquad (9)$$

where a and t are constants associated with initial and final operational bounds, and $\alpha \in R$ (R is the set of real numbers) is the fractional order of the integro-differential operator.

There are many applicable definitions available in the literature describing the fractional derivative function, but the mostly applied one pertains to the Riemann–Liouville (RL) definition. In this definition, fractional derivative of order α of a function $f(t)$ is given by

$$_aD_t^\alpha f(t) = \frac{1}{\Gamma(n-\alpha)} \frac{\mathrm{d}^n}{\mathrm{d}t^n} \int_a^t \frac{f(\tau)}{(t-\tau)^{\alpha-n+1}} \mathrm{d}\tau \qquad (10)$$

where $n - 1 < \alpha < n$, n is the integer part of α, $n \in N$ and $\Gamma(\cdot)$ is the Euler's gamma function given by

$$\Gamma(s) = \int_0^\infty t^{s-1} e^{-s} \mathrm{d}t, \quad s > 0 \qquad (11)$$

$\Gamma(s + 1)$ is equal to $s!$, when s is an integer.

For convenience, the Laplace domain transformation is used to portray the fractional integro-differential process. The Laplace transformation of Eq. 10 under zero initial condition for the fractional derivative can be written as

$$\mathcal{L}\{_aD_t^\alpha f(t)\} = \int_0^\infty e_a^{-st} D_t^\alpha f(t) \mathrm{d}t$$
$$= s^\alpha F(s) - \sum_{k=0}^{n-1} s_a^k D_t^{\alpha-k-1} f(t)|_{t=0} \qquad (12)$$

for $n - 1 < \alpha < n$ while $F(s) = \mathcal{L}\{f(t)\}$ signifies the normal Laplace transformation.

FOPID is often referred to as $PI^\lambda D^\mu$ controller, where λ and μ are the non-integer orders of integral and derivative parts and can be any real numbers. Owing to the addition of tunable λ and μ parameters, controllers composing of different combinations of proportional, integral and/or derivative control action become more flexible and robust while at the same time the system performance could be also boosted, but their design is more complex than their integer order counterpart. Fractional order differential equation of a control system can be given by

$$b_m D^{\beta_m} y(t) + \cdots + b_1 D^{\beta_1} y(t) + b_0 D^{\beta_0} y(t)$$
$$= a_n D^{\alpha_n} u(t) + \cdots + a_1 D^{\alpha_1} u(t) + a_0 D^{\alpha_0} u(t) \qquad (13)$$

where $u(t)$ and $y(t)$ are input and output (state) signals, respectively. $D^{\alpha_n} \equiv {}_0D_t^{\alpha_n}$ and $D^{\beta_n} \equiv {}_0D_t^{\beta_n}$ symbolize a

fractional order operator under zero initial condition, a_i ($i = 0, 1, 2,\ldots, n$) and b_j ($j = 0, 1, 2,\ldots, m$) are arbitrary constants, α_i ($i = 0, 1, 2,\ldots, n$) and β_j ($j = 0, 1, 2,\ldots, m$) are random real numbers. Assuming the inequalities are $\alpha_n > \alpha_{n-1} > \cdots > \alpha_0 \geq 0$ and $\beta_n > \beta_{n-1} > \cdots > \beta_0 \geq 0$, the transfer function of Eq. 13 in s-domain can be derived by Eq. 14 with initial conditions of $[{}_0D_t^{\alpha_i-i-1} y(t)]_{t=0}$ ($i = 0, 1, 2,.., n - 1$) and $[{}_0D_t^{\beta_j-j-1} y(t)]_{t=0}$ ($j = 0, 1, 2,\ldots, m - 1$).

$$G(s) = \frac{Y(s)}{U(s)} == \frac{a_n s^{\alpha_n} + a_{n-1} s^{\alpha_{n-1}} \cdots + a_1 D^{\alpha_1} + a_0 D^{\alpha_0}}{b_m s^{\beta_m} + b_{m-1} s^{\beta_{m-1}} \cdots + b_1 s^{\beta_1} + b_0 D^{\beta_0}} \qquad (14)$$

And one arrives at the following transfer function form of FOPID controller:

$$G_{\mathrm{FOPID}}(s) = K_p + \frac{K_i}{s^\lambda} + K_d s^\mu, \quad (\lambda, \mu > 0) \qquad (15)$$

In Eq. 15, K_p, K_i and K_d are proportional, integral and derivative gains, respectively, and λ and μ are liable for order of integration and differentiation. As such, there are five independent parameters to be tuned prior to operation with a FOPID controller. In guidance of Eq. 15, Table 1 is provided to observe the resulting controller structure depending upon the settings of λ and μ. It is clear from this table that all the classical versions of the PID controller are associated with the unique cases of the fractional $PI^\lambda D^\mu$ controller. For example, if λ and μ are both set to 1, the resulting controller structure is a conventional integer order PID controller. Similarly, if $\mu = 0$, it becomes PI^λ, and if $\lambda = 0$, it becomes PD^μ.

In computer simulations and real-time implementations of transfer functions including fractional powers of s, it is needed to approximate them with usual integer order transfer functions. To do this properly, a usual transfer function would normally include an infinite number of poles and zeroes. But, approximating with a finite number of poles and zeroes is also possible using the CRONE approximation concept suggested by Oustaloup who uses recursive distribution of N real poles and N real zeroes (Oustaloup et al. 2000). The Oustaloup filter given by Eq. 16 is known to provide a very good approximation/matching with the fractional order elements s^α within a chosen frequency band $[\omega_L, \omega_H]$ and order N (Pan and Das 2015).

$$G_f(s) = s^\alpha = K \prod_{k=-N}^{N} \frac{s + \omega_k^z}{s + \omega_k^p} \qquad (16)$$

where K is the filter gain, ω_k^z and ω_k^p are the zeroes and poles of $G_f(s)$ calculated by

Table 1 Controller structure with varying λ and μ

No.	Integrator order	Differentiator order	Resulting controller structure
1	λ	μ	$PI^{\lambda}D^{\mu}$
2	1	1	PID
3	1	0	PI
4	0	1	PD
5	0	0	P
7	λ	0	PI^{λ}
8	0	μ	PD^{μ}
9	1	μ	PID^{μ}
10	λ	1	$PI^{\lambda}D$

$$K = \omega_H^{\alpha} \tag{17}$$

$$\omega_k^z = \omega_L \left(\frac{\omega_H}{\omega_L} \right)^{\frac{k+N+0.5(1-\alpha)}{2N+1}} \tag{18}$$

$$\omega_k^p = \omega_L \left(\frac{\omega_H}{\omega_L} \right)^{\frac{k+N+0.5(1+\alpha)}{2N+1}} \tag{19}$$

There are two crucial parameters, filter gain K and approximation order N, having notable influence on the performance of this approximation. K is tuned so that the gain of the approximation should be unity at 1 rad/s frequency. Low value of N gives rise to simpler approximation and ease from the practical point of view but the approximation performance decays owing to ripple formation in magnitude and phase response. Such problem can be resolved by increasing N, but it will make the approximation complicated and computationally painful in real-time experimentation. Thus, considering the trade-off between the precision and complexity, CRONE approximation is realized in this paper with $N = 3$ and fitting frequency range equal to $[10^{-2}, 10^2]$ rad/s.

3.2 Proposed FOPI–FOPD cascade controller

To advance LFC performance in a wide range of EPSs, FOPI–FOPD cascade controller is proposed in this paper. To the author's knowledge, the designed controller is unique, and has not been employed in LFC studies previously. Thus, its application in the field is a research avenue and improving the system performance by using FOPI–FOPD cascade controller will also be the valuable contributions of the present paper. The block diagram of this controller structure is illustrated in Fig. 5.

As perceived in Fig. 5, the proposed controller involves two controllers namely FOPI and FOPD connected in cascade. By receiving the ACE signal, the FOPI controller generates a signal, which also acts as input of the FOPD controller. The output of the FOPI–FOPD cascade controller is the reference power setting or control input i.e.

ΔP_{ref} for the EPSs to be controlled as mathematically given by Eq. 20.

$$\Delta P_{\text{ref}} = \text{ACE} \cdot \overbrace{\left(K_{p1} + K_i s^{-\lambda} \right)}^{\text{FOPI}} \cdot \overbrace{\left(K_{p2} + K_d s^{\mu} \right)}^{\text{FOPD}} \tag{20}$$

For $\lambda = 1$ and $\mu = 1$, the FOPI–FOPD cascade controller turns into a simpler form of classical PI–PD cascade controller. The red faced variables highlighted in Fig. 5, i.e. K_{p1}, K_{p2}, K_i, K_d, λ and μ, are six unknown design parameters to be optimized. Due to the extra two degrees of freedom resulting from the orders of integrator and differentiator, newly structured FOPI–FOPD cascade controller is expected to better cope with the dynamical properties of LFC problem compared to conventional PI–PD cascade controller.

Prior to the FOPI–FOPD cascade controller's design, we had three goals. Firstly, it should be cost-effective, simple and easy from the perspectives of design and implementation. Thus, the controller has the PID-like control action. Secondly, PI and PD controllers are cascaded, i.e. PI–PD to blend the advantages of distinct features and strengths of the two controllers. On the other hand, in a cascade controller, there are more tuning knobs than a non-cascade controller and it is known that if there are more tuning knobs, improved system performance may be obtained from that controller. Moreover, the cascade control is popular for its quick disturbance rejection ability before it effuses to the other parts of the system. To add more flexibility to controller design and cultivate PI–PD cascade controller performance, it is considered with fractional integrator/derivative order, i.e. FOPI–FOPD in order to fulfill our third aim.

3.3 Optimization of FOPI–FOPD cascade controller

To gain success from the FOPI–FOPD cascade controller to the maximum extent possible, its parameters such as K_{p1}, K_{p2}, K_i, K_d, λ and μ are required to be optimized concurrently. The role of an optimization progress is to find

Fig. 5 Block diagram of FOPI–FOPD cascade controller structure
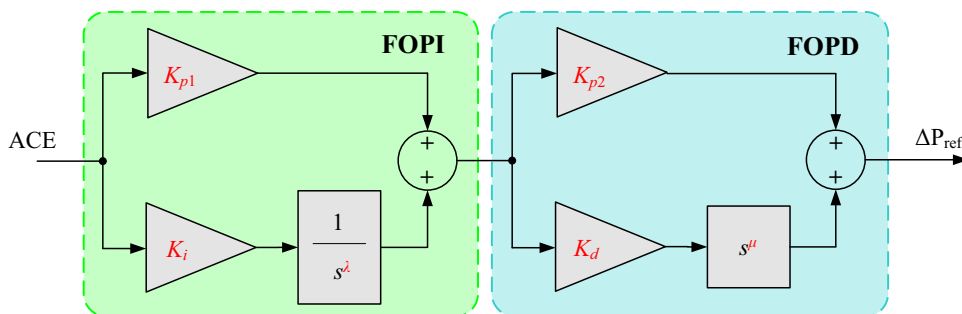
the most promising solution in a feasible region by minimizing a cost function. The choice of this function is specific to the problem at hand and it has a strong impact over the system dynamic behavior. In the present work, ITAE criterion is assumed as cost function (J_{ITAE}) to be utilized in the controller optimization task. J_{ITAE} declared via Eqs. 21–23 for single-area, two-area and three-area EPSs is the classical one and widely employed in other published works. Compared with other error integrating alternatives, ITAE is recognized to bestow superior results in LFC field (Sivalingam et al. 2017; Sahu et al. 2015).

$$J_{\text{ITAE}} = \int_0^{t_{\text{sim}}} t|\Delta f|\mathrm{d}t \quad \text{for single area EPS} \tag{21}$$

$$J_{\text{ITAE}} = \int_0^{t_{\text{sim}}} t(|\Delta f_1| + |\Delta f_2| + |\Delta P_{\text{tie}}|)\mathrm{d}t \tag{22}$$

for two - area EPS

$$J_{\text{ITAE}} = \int_0^{t_{\text{sim}}} t(|\Delta f_1| + |\Delta f_2| + |\Delta f_3| + |\Delta P_{\text{tie1}}| + |\Delta P_{\text{tie2}}|$$

$$+ |\Delta P_{\text{tie3}}|)\mathrm{d}t \quad \text{for three - area EPS} \tag{23}$$

where t_{sim} is the time horizon of simulation. Consequently, the FOPI–FOPD cascade controller design problem can be formulated as the subsequent optimization problem subject to linear inequalities of the controller parameters bounds:

$$
\begin{aligned}
K_{p1}^{\min} &\leq K_{p1} \leq K_{p1}^{\max} \\
K_{p2}^{\min} &\leq K_{p2} \leq K_{p2}^{\max} \\
K_i^{\min} &\leq K_i \leq K_i^{\max} \\
K_d^{\min} &\leq K_d \leq K_d^{\max} \\
\lambda^{\min} &\leq \lambda \leq \lambda^{\max} \\
\mu^{\min} &\leq \mu \leq \mu^{\max}
\end{aligned}
\tag{24}
$$

where the superscripts min and max are the minimum and maximum values of FOPI–FOPD cascade controller gains, respectively. There is no certain way to decide these values

at design stage of a controller. The task becomes more problematic when introducing a new controller. To ensure both EPS stability and fruitful optimization process, we decide the ranges in this work as follows: the minimum and maximum values for $K_{p1,p2,i,d}$ are selected as 0.0 and 3.0 for test systems 1, 2 and 3, whereas the respective range is set between -2 and 2 for test systems 4 and 5. However, λ and μ values are chosen between 0.0 and 1.5 for all test systems. To enrich EPS dynamic performance, DSA is allowed to search for optimal gain values of FOPI–FOPD cascade controller within this specified range to minimize J_{ITAE}.

4 Dragonfly search algorithm

Inspecting the literature reveals that the employment of DSA in optimization of controller parameters for LFC of EPS is very limited (Venkatesh and Sudheer 2017; Nour et al. 2018). So, this study is devoted to investigate the capabilities of DSA more thoroughly for proper gain adjustment of the designed controller in presence of different kinds of EPSs. DSA has been recently proposed by Seyedali as an alternative and powerful optimizer to solve some optimization problems that could not be solved by other available algorithms (Seyedali 2016). It is a bioinspired metaheuristic search technique based on the computer programming of identified individual and swarm intelligence of a fancy insect called dragonfly. As shown in Fig. 6, dragonflies have a long thin body with two pairs of large transparent wings that sprawl sideways at rest. This way, they can fly fast and hunt most of other small insects living in nature.

There are two essential milestones in the lifecycle of a dragonfly: nymph and adult. The significant portion of their lifespan is spent in nymph and then they undergo a metamorphosis with a series of nymphal phases from which the adult appears. Interestingly, the swarming behavior of dragonflies is genuine and rare in nature. They swarm for two objectives only: hunting and migration, which are named as static (feeding) swarm and dynamic (migratory) swarm, respectively (Seyedali 2016). In a static swarm,

Fig. 6 Photography of a dragonfly

small sub-swarms are created and dragonflies in these swarms are flied over different areas. Localized movements and sudden changes are the salient properties of this swarm. In a dynamic swarm, however, a greater number of dragonflies form the swarm so as to migrate alongside one direction over long distances. As such, so-called static and dynamic swarming behaviors are the fundamentals of DSA operation and they are very familiar with two important characteristics of metaheuristic search algorithms: exploration (diversification) and exploitation (intensification). Static swarm tries to emphasize on exploration while dynamic swarm provides the algorithm with exploitation. Mathematical modeling of these two phases is described as stepdown.

To maintain surviving, individuals in any swarm should move toward food sources and distract the enemy's attention from giving harms to themselves. Taking these two behaviors into account, position updating of individuals in swarms is done by five factors such as (1) separation, (2) alignment, (3) cohesion, (4) attraction to food, and (5) distraction from enemy. The following describes each of these behaviors mathematically.

1. Separation

The separation is computed by Eq. 25.

$$S_i = -\sum_{j=1}^{N} X - X_j \tag{25}$$

where X is the position of the current individual, X_j speaks for the jth individual in the neighborhood and N is the count of neighboring individuals.

2. Alignment

Alignment can be computed by the following expression.

$$A_i = \frac{\sum_{j=1}^{N} V_j}{N} \tag{26}$$

where V_j shows the velocity of jth neighboring individual.

3. Cohesion

Cohesion is represented as follows.

$$C_i = \frac{\sum_{j=1}^{N} X_j}{N} - X \tag{27}$$

4. Attraction toward food source

This behavior is mathematically given by Eq. 28 with X^+ being the position of a food source.

$$F_i = X^+ - X \tag{28}$$

5. Distraction from enemy

Mathematical concept for such a distraction outwards from an enemy is presented in Eq. 29 with X^- being the position of the enemy.

$$E_i = X^- + X \tag{29}$$

In DSA, the behavior of dragonflies is considered dependent on the weighted combination of these five types of attitudes. To update the position of dragonflies and mimic their movements in a search space, two vectors, namely step (ΔX) and position (X), are generated. The former is developed analogous to the velocity vector in PSO. The step vector is liable for the movement direction of dragonflies and represented by

$$\Delta X_{t+1} = (sS_i + aA_i + cC_i + fF_i + eE_i) + w\Delta X_t \tag{30}$$

where s, a, c, f and e are the weights of the corresponding behaviors, i is for the ith individual, w is the inertia weight, and t is the current iteration.

After calculating the step vector, the position vector is calculated in the same way PSO uses as depicted in Eq. 31.

$$X_{t+1} = X_t + \Delta X_{t+1} \tag{31}$$

Using different separation, alignment, cohesion, food and enemy factors (s, a, c, f, and e), it is possible in DSA to achieve different explorative and exploitative behaviors during the course of optimization. Dragonflies' neighbors are also very significant, so a neighborhood with a particular radius is considered around every dragonfly in DSA. Given this, by increasing the radii of neighboring solutions proportional to the number of iterations, transitions between exploration and exploitation can be made in the algorithm. Another way to have a good balance between exploration and exploitation is to tune the swarming factors

$(s, a, c, f$ and $e)$ besides the inertia weight (w) adaptively during optimization.

To enhance the randomness, stochasticity and explorative behavior of the artificial dragonflies once no neighboring solutions exist, a random walk (Lévy flight) is employed in DSA using the following expression.

$$X_{t+1} = X_t + \text{Le vy}(d)\Delta X_t \tag{32}$$

where t is the current iteration, d is the dimension of the position vector, and Lévy flight is:

$$\text{Levy}(x) = 0.01 \cdot \frac{r_1 \cdot \sigma}{|r_2|^{1/\beta}} \tag{33}$$

In Eq. 33, r_1 and r_2 are random numbers in the range [0, 1], β is a constant, and σ is derived using the following formula.

$$\sigma = \left(\frac{\Gamma(1 + \beta) \cdot \sin\left(\frac{\pi\beta}{2}\right)}{\Gamma\left(\frac{1+\beta}{2}\right) \cdot \beta \cdot 2^{\left(\frac{\beta-1}{2}\right)}} \right)^{1/\beta} \tag{34}$$

where $\Gamma(x) = (x - 1)!$.

For convenience, the pseudocode representation of DSA is depicted in Algorithm 1.

Algorithm 1: Pseudocode representation of DSA

instead design a unique control scheme for supplementary controller that has not been considered so far in LFC studies. For proper gain adjustment, we prefer the DSA technique as a means to other existing metaheuristics owing to its promising features depicted above and its rare application to address LFC problem. For further details and descriptive figures of DSA, the readers are kindly advised to refer the DSA's original paper (Seyedali 2016).

5 Simulated results and discussion

To recognize the ability and efficacy of DSA tuned FOPI–FOPD cascade controller, MATLAB/Simulink software version 9.3.0 (2017b) is used to simulate the EPS models under study and obtain the dynamic responses of the systems for a variety of operating scenarios. The simulation sampling-interval is tuned to $T_s = 1$ ms. The magnitude and location of SLP are selected basing on the works benchmarked for a fair comparison. The tolerance band for calculating settling time T_s of the responses is defined as 2% of the given SLP for all EPS models in the current study, i.e. if SLP is assumed as 1%, then T_s is calculated in tolerance band of $\pm0.02 \times 0.01 = \pm0.0002$. The time

---

Algorithm 1: Pseudocode representation of DSA

Initialize a population with a number of random dragonflies X_i $(i = 1, 2, .., n)$
Initialize step vectors ΔX_i $(i = 1, 2, .., n)$
while *termination criteria not satisfied*
    Compute the fitness values of all dragonflies
    Update the positions of food source X^+ and enemy X^-
    Update tunable parameters s, a, c, f, e, w
    Compute S, A, C, F, E using Eqs. 25-29
    Update neighborhood radius
    if a dragonfly has at least one dragonfly in the neighborhood
        Compute velocity vector by Eq. 30
        Update position vector by Eq. 31
    else
        Update position vector by Eq. 32
    end
    Assess the new positions and correct if violating the variable boundaries
end
Save the best dragonfly for use in simulations

The results reported in (Seyedali 2016) proved that DSA is able to offer high exploration and high exploitation thanks to its efficient search model based on the identified static and dynamic swarming behaviors of dragonflies. Implementation of such behaviors is easy with only simple mathematical operations to code. Yet it is important to emphasize that DSA and/or its modified version is not the main focus of this paper, but our main contribution is to

range considered for the computation of J_{ITAE} is the simulation time shown on the plots. The optimizer, DSA, is run in an *.m.file* script and this file is connected to the Simulink environment for cost function evaluation. According to the results obtained from experiments made on five simulated EPSs, the results in this section have been analyzed in four subsections. In each subsection, a number of studies that we believe are able to challenge the designed controller

Table 2 Optimized controller parameters and T_s/J_{ITAE} results of test system-1

Controllers/parameters	BFOA: PI (Ali and Abd-Elazim 2011)	hBFOA-PSO: PI (Panda et al. 2013)	DE: PI (Rout et al. 2013)	TLBO: PID (Sahu et al. 2016)	TLBO: 2DOF PID (Sahu et al. 2016)	hPSO-PS: fuzzy PID (Sahu et al. 2015)	ISFS: PID (Çelik 2020)	DSA: FOPID	DSA: FOPI–FOPD
Controller parameters	$K_p = -0.4207$ $K_i = 0.2795$	$K_p = -0.4383$ $K_i = 0.3349$	$K_p = -0.2146$ $K_i = 0.4345$	$K_p = 1.1726$ $K_i = 1.9370$ $K_d = 1.1635$	$K_p = 1.8920$ $K_i = 1.7471$ $K_d = 0.2266$ $N = 112.8251$ $PW = 0.4839$ $DW = 1.1207$	$K_1 = 0.9852$ $K_2 = 0.5595$ $K_p = 0.9336$ $K_i = 0.7203$	$K_p = 1.6293$ $K_i = 2.0000$ $K_d = 0.5882$	$K_p = 2.0331$ $K_i = 2.9999$ $K_d = 0.4670$ $\lambda = 1.0007$ $\mu = 1.0517$	$K_{p1} = 1.2485$ $K_{p2} = 2.9999$ $K_i = 2.9998$ $K_d = 3.0000$ $\lambda = 1.1007$ $\mu = 0.6312$
T_s (s) (2% band)									
Δf_1	5.52	5.17	8.96	4.84	2.41	2.26	2.15	1.13	0.72
Δf_2	7.09	6.81	8.16	5.13	2.13	3.74	3.66	2.73	1.48
ΔP_{tie}	6.35	4.59	5.75	3.03	2.56	2.94	3.01	2.23	0.86
J_{ITAE}	1.8270	n/a	0.9911	0.2452	0.0269	0.1438	n/a	0.0778	0.0180
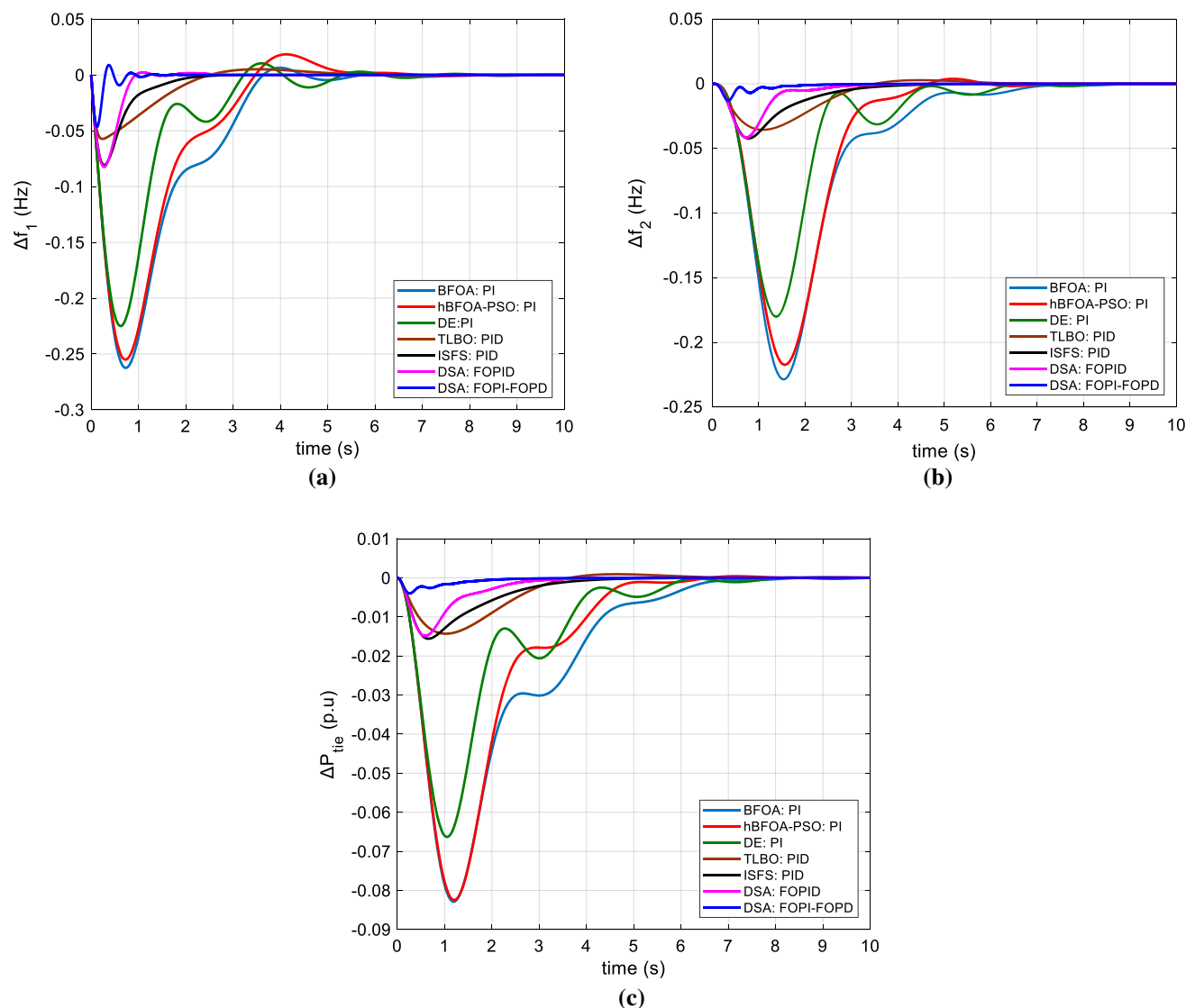
Fig. 7 Comparison of time-domain responses for test system-1 after a 10% SLP in area-1 **a** Δf_1 **b** Δf_2 **c** ΔP_{tie}

have been chosen for comparison to check how competitive the proposed approach is. In DSA, the population size (number of search agents) is 50 and the number of iterations is tuned to 50. Optimization process with DSA is repeated 30 times for each model and the final best solution over 30 runs is set as the controller parameters used in simulations.

5.1 Two-area non-reheat thermal power system

The model of this system is shown in Fig. 1a and the relevant system parameters can be found in "Appendix A.1" section. Each area, rigged by FOPI–FOPD cascade controller, has one generating unit based on non-reheat thermal plant. The parameters of FOPID and cascade FOPI–FOPD controllers are optimized by DSA and J_{ITAE}

considering a 10% SLP at $t = 0$ in area-1. The final controller parameters along with T_s/J_{ITAE} results of frequency and tie-line power deviations are displayed in Table 2. For comparison purpose, the respective data offered by other recent studies based on BFOA (Ali and Abd-Elazim 2011), hBFOA-PSO (Panda et al. 2013) and DE (Rout et al. 2013) optimized PI controllers, PID and 2DOF controllers tuned by teaching learning-based optimization (TLBO) algorithm (Sahu et al. 2016), hybrid PSO and pattern search (PS) optimized fuzzy PID controller (Sahu et al. 2015) and improved stochastic fractal search (ISFS) algorithm-based PID controller (Çelik 2020) is also gathered in Table 2. An entry given by "n/a" in any of the following tables means not available. It is notable in Table 2 that DSA tuned FOPI–FOPD cascade controller is superior to all the techniques

Table 3 Optimized controller parameters and T_s/J_{ITAE} results of test system-2

Controllers/parameters	hBFOA-PSO: PI (Panda et al. 2013)	hPSO-PS: fuzzy PID (Sahu et al. 2015)	CRAZYPSO: PI (Gozde and Taplamacioglu 2011)	DE: PID (Mohanty et al. 2014)	ISFS: PID (Çelik 2020)	DSA: FOPID	DSA: FOPI–FOPD
Controller parameters	$K_p = -0.5484$ $K_i = 0.2277$	$K_1 = $ n/a $K_2 = $ n/a $K_p = $ n/a $K_i = $ n/a	$K_p = -0.5762$ $K_i = 0.1962$ $w_1 = 0.7300$ $w_2 = 0.6848$ $w_3 = 0.7879$	$K_p = 0.2383$ $K_i = 0.9718$ $K_d = 0.4922$	$K_p = 0.3898$ $K_i = 1.0113$ $K_d = 0.7695$	$K_p = 2.5578$ $K_i = 2.9999$ $K_d = 0.7937$ $\lambda = 1.0020$ $\mu = 1.2510$	$K_{p1} = 2.3181$ $K_{p2} = 2.9999$ $K_i = 2.9879$ $K_d = 0.4391$ $\lambda = 1.0000$ $\mu = 1.4642$
T_s (s) (2% band)							
Δf_1	10.85	10.11	11.08	6.87	6.25	2.34	1.22
Δf_2	10.95	10.13	11.99	6.89	6.48	3.63	2.25
ΔP_{tie}	9.43	9.01	11.12	4.40	4.40	2.33	1.05
J_{ITAE}	n/a	0.3471	n/a	n/a	n/a	0.0121	0.0034

as minimum J_{ITAE} value ($J_{ITAE} = 0.0180$) is achieved compared to BFOA ($J_{ITAE} = 1.8270$), DE ($J_{ITAE} = 0.9911$) tuned PI controller, TLBO tuned PID controller ($J_{ITAE} = 0.2452$), TLBO tuned 2DOF PID controller ($J_{ITAE} = 0.0269$), hPSO-PS tuned fuzzy PID controller ($J_{ITAE} = 0.1438$) and DSA tuned FOPID controller ($J_{ITAE} = 0.0778$). This accordingly bestows that the proposed approach reaches better performance since minimum settling times of frequency and tie-line power deviations are obtained compared to other indicated solutions. Considering the settling times of Δf_1 and ΔP_{tie} signals, the second best performer in this case is DSA tuned FOPID controller. Here, it is worth mention that hBFOA-PSO algorithm uses a more comprehensive cost function with three goals: minimizing ITAE, maximizing the minimum damping ratio and minimizing the settling times of Δf_1, Δf_2, and ΔP_{tie} signals. Similarly, ISFS optimizes the ITAE of frequency and tie-line power deviations, and also the time rates of changes in these deviations, causing a process of computationally expensive cost function calculation.

The comparative time-domain system responses after a 10% SLP at $t = 0$ in area-1 are illustrated in Fig. 7, from which the settling times reported in Table 2 are measured considering a tolerance band of $\pm$ 0.002. Notice that the responses with 2DOF PID and fuzzy PID controller are not shown in Fig. 7 because the respective controllers could not be designed due to their complex structures. The simulated results presented here show that the steady state performance is the same for all the controllers since frequency deviation of each area and tie-line power deviation ceases to zero in the steady state. However, there are

notably significant differences in their transient responses. As seen, the response with DSA optimized FOPI–FOPD cascade controller is the pioneer of the other approaches since it is driven back to zero hastily after a far smaller peak undershoot. This is followed by the response with DSA tuned FOPID controller.

5.2 Two-area non-reheat thermal power system with GDB nonlinearity

To access the effectiveness of DSA tuned FOPI–FOPD cascade controller in a more realistic case, the nonlinear model of two-area non-reheat thermal EPS exploiting the nonlinear source of governor dead band (GDB) nonlinearity is investigated in this section. Transfer function model of this system is shown in Fig. 1b and the nominal system parameters are given in "Appendix A.2" section. The controller parameters are optimized when there is a SLP of 1% applied to area-1 at $t = 0$. The optimized controller parameters and the corresponding system results are reported in Table 3. To demonstrate the supremacy of our proposal, results of DSA optimized FOPID controller along with other well-regarded studies such as hBFOA-PSO (Panda et al. 2013) and CRAZYPSO algorithm (Gozde and Taplamacioglu 2011) optimized PI controllers, DE (Mohanty et al. 2014) and ISFS (Çelik 2020) optimized PID controllers and hPSO-PS tuned fuzzy PID controller (Sahu et al. 2015) for the identical EPS are also provided in Table 3. Note that CRAZYPSO and DE-based approaches adopt different and more complex cost functions compared to the J_{ITAE} itself. It is noticeable from Table 3 that the J_{ITAE} value
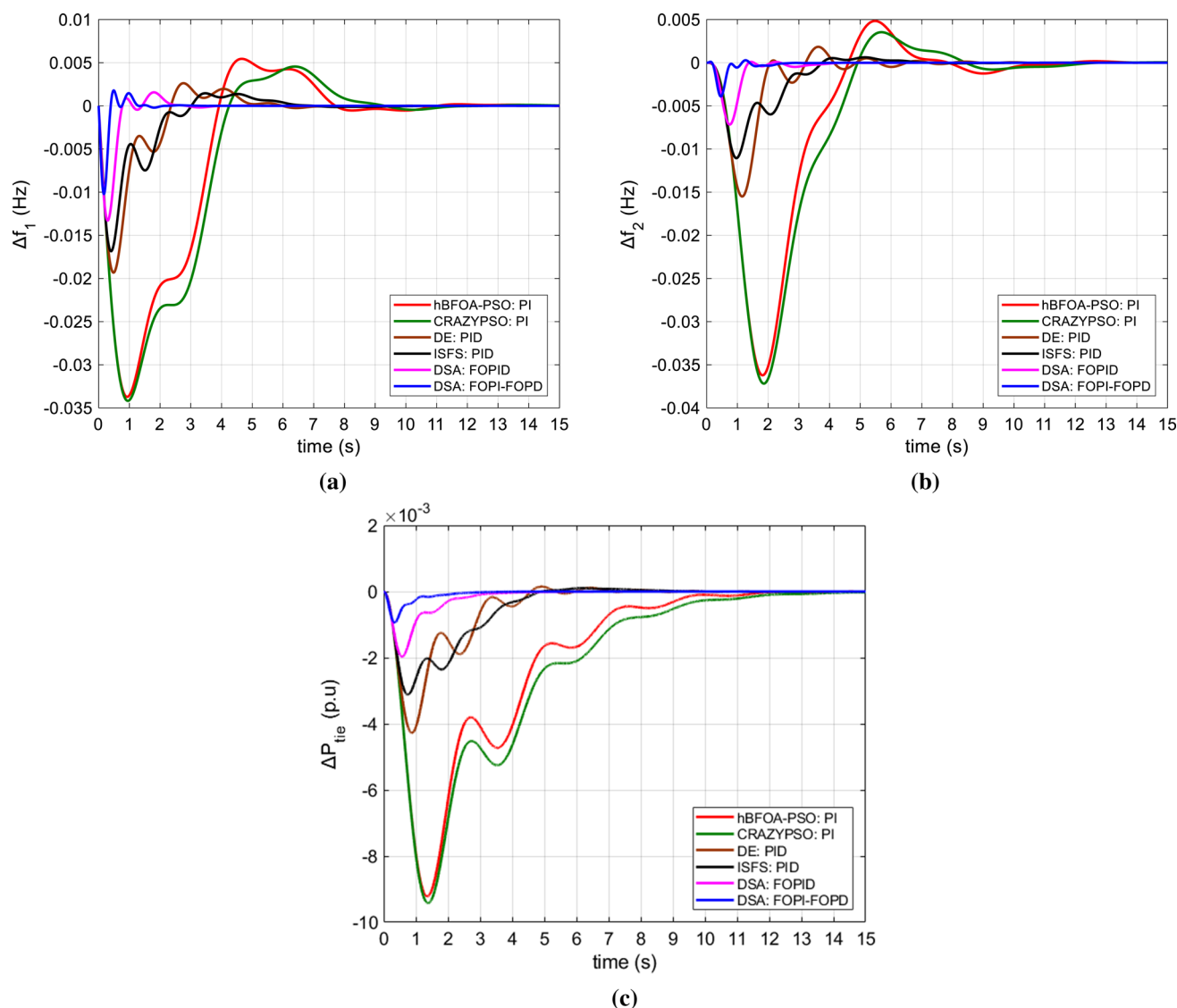
Fig. 8 Comparison of time-domain responses for test system-2 after a 1% SLP in area-1 **a** Δf_1 **b** Δf_2 **c** ΔP_{tie}

offered by DSA tuned FOPI–FOPD cascade controller is $J_{\text{ITAE}} = 0.0034$, which is smaller than that by DSA tuned FOPID ($J_{\text{ITAE}} = 0.0121$) and hPSO-PS tuned fuzzy PID ($J_{\text{ITAE}} = 0.3471$) controllers. It is also clear from Table 3 that settling times of Δf_1, Δf_2, and ΔP_{tie} signals with the proposed method are notably improved compared to all other approaches.

The comparative time-domain system responses are given in Fig. 8. It can be seen from Fig. 8 that the SLP in area-1 is rejected very fast in presence of the proposed controller. Thus, the oscillations and time-domain characteristics like settling time/undershoot/overshoot, which are observed to be severe in the existing solutions, are reduced effectively. The second best performance for this system belongs to the DSA tuned FOPID controller.

5.3 Three-area hydrothermal power system with GRC

The model of this system is depicted in Fig. 2 and the applicable system parameters are provided in "Appendix A.3" section. The controller parameters are optimized using DSA by minimizing J_{ITAE} when a 1% SLP has been enforced in all the three areas simultaneously at $t = 0$. The optimized gains of FOPI–FOPD cascade controller and the corresponding system results are tabulated in Table 4. To highlight the controller talent, the obtained results are contrasted with the results of DSA optimized FOPID controller, integral controller (Nanda et al. 2006), hBFOA-PSO optimized PI (Panda et al. 2013) and ISFS optimized PID (Çelik 2020) controllers for the same EPS. From Table 4, it is obvious that DSA optimized FOPI–FOPD

Table 4 Optimized controller parameters and T_s/J_{ITAE} results of test system-3

Algorithm	Integral (Nanda et al. 2006)	hBFOA-PSO: PI (Panda et al. 2013)	ISFS: PID (Çelik 2020)	DSA: FOPID	DSA: FOPI-FOPD
Controller parameters	**Area 1: Thermal** $K_i = 0.111$ **Area 2: Thermal** $K_i = 0.111$ **Area 3: Hydro** $K_i = 0.027$	**Area 1: Thermal** $K_p = -0.1502$ $K_i = 0.0952$ **Area 2: Thermal** $K_p = -0.1202$ $K_i = 0.1199$ **Area 3: Hydro** $K_p = -0.0399$ $K_i = 0.021$	**Area 1: Thermal** $K_p = 1.1539 \times 10^{-12}$ $K_i = 0.0577$ $K_d = 0.1606$ **Area 2: Thermal** $K_p = 1.1539 \times 10^{-12}$ $K_i = 0.0577$ $K_d = 0.1606$ **Area 3: Hydro** $K_p = 1.1539 \times 10^{-12}$ $K_i = 0.0577$ $K_d = 0.1606$	**Area 1: Thermal** $K_p = 0.0001$ $K_i = 0.1253$ $K_d = 0.1206$ $\lambda = 1.0000$ $\mu = 0.5004$ **Area 2: Thermal** $K_p = 0.0001$ $K_i = 0.1253$ $K_d = 0.1206$ $\lambda = 1.0000$ $\mu = 0.5004$ **Area 3: Hydro** $K_p = 0.0001$ $K_i = 0.0264$ $K_d = 0.0350$ $\lambda = 1.0000$ $\mu = 0.7376$	**Area 1: Thermal** $K_{p1} = 0.0316$ $K_{p2} = 0.3346$ $K_i = 0.3424$ $K_d = 0.0271$ $\lambda = 1.0000$ $\mu = 0.6354$ **Area 2: Thermal** $K_{p1} = 0.0316$ $K_{p2} = 0.3346$ $K_i = 0.3424$ $K_d = 0.0271$ $\lambda = 1.0000$ $\mu = 0.6354$ **Area 3: Hydro** $K_{p1} = 0.0001$ $K_{p2} = 0.0001$ $K_i = 0.2249$ $K_d = 0.0396$ $\lambda = 1.4999$ $\mu = 0.0100$
T_s (s) (2% band)					
Δf_1	147.8	171.1	107.6	137.5	90.3
Δf_2	147.8	171.1	107.6	137.5	90.3
Δf_3	147.8	171.1	107.6	137.6	90.0
ΔP_{tie1}	119.1	131.5	65.28	109.1	68.7
ΔP_{tie2}	119.1	133.5	65.28	109.1	68.7
ΔP_{tie3}	139.7	163.6	94.83	130.9	74.7
J_{ITAE}	n/a	n/a	n/a	156.32	147.56

cascade controller achieves smaller value of J_{ITAE} ($J_{ITAE} = 147.56$) than DSA optimized FOPID controller ($J_{ITAE} = 156.32$), verifying that FOPI–FOPD cascade controller outperforms FOPID controller in this scenario. Also, taking the settling times of ΔP_{tie1} and ΔP_{tie2} responses the same for ISFS optimized PID and DSA optimized cascade FOPI–FOPD controllers, DSA optimized FOPI–FOPD cascade controller is the most promising controller and yields to significant reduction in settling time in comparison with other approaches.

The system dynamic responses are comparatively shown in Fig. 9. Employing the proposed controller, the magnitude of sustained oscillations initially observed is suppressed hastily with time, permitting the responses to converge very early to the reference zero steady state value. As a result, DSA tuned FOPI–FOPD cascade controller is found capable of acting skillfully in multi-area EPS with disruptive effect of GRC.

5.4 Extension to multi-source power system

a. Multi-source single-area power system

At the first instant, performance comparisons are investigated on multi-source single-area EPS depicted in Fig. 3. Participation factors of generating sources of thermal, hydro and gas units are set to 55%, 32% and 12%, respectively, in parallel with the literature works. Other system parameters are given in "Appendix A.4" section. To better illustrate the advanced tuning performance of proposed DSA technique over the other existing algorithms such as optimal output feedback controller (Parmar et al. 2012), DE (Mohanty et al. 2014), TLBO (Barisal

(a) **(b)** **(c)** **(d)** **(e)** **(f)**
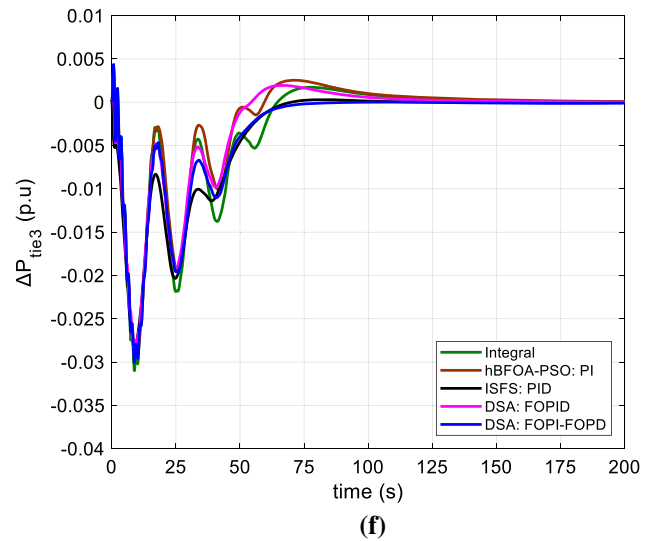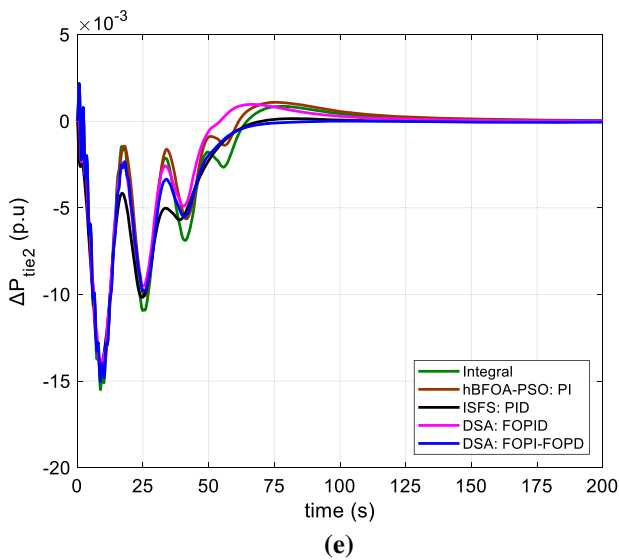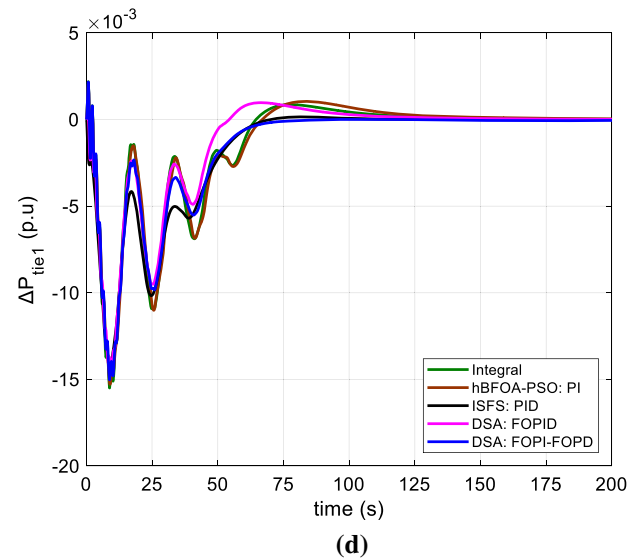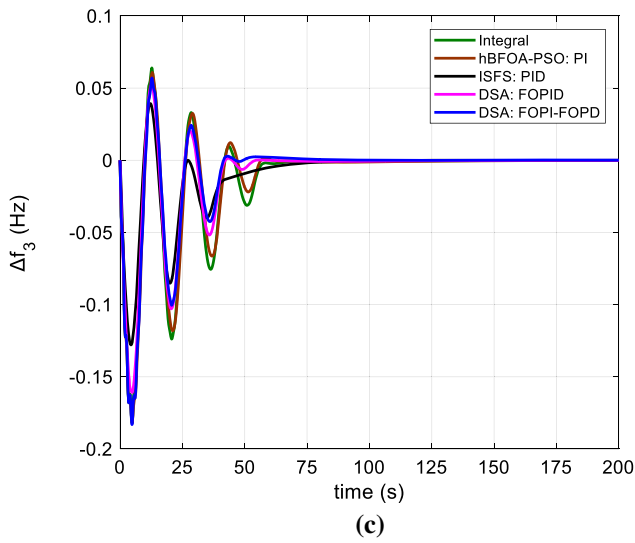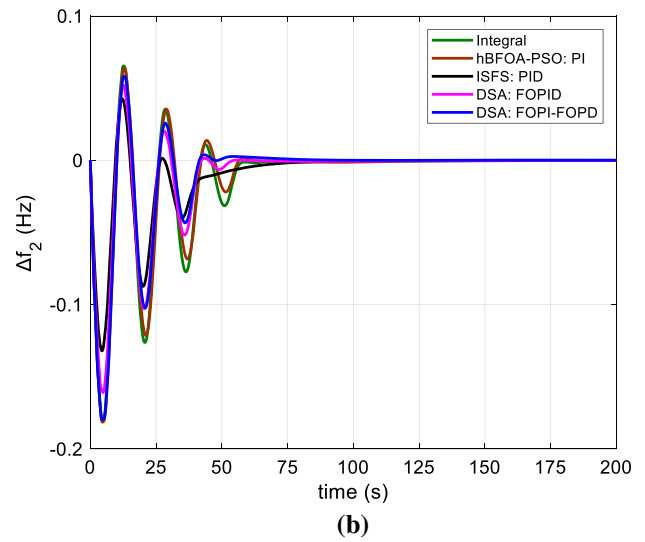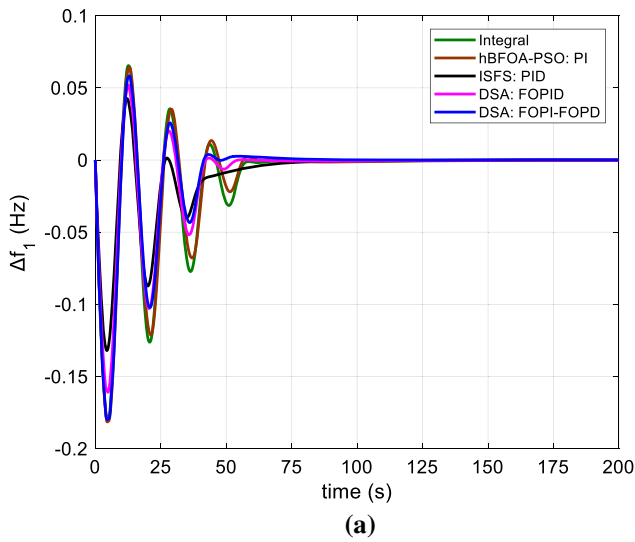
◄**Fig. 9** Comparison of time-domain responses for test system-3 after a 1% SLP in all areas **a** Δf_1 **b** Δf_2 **c** Δf_3 **d** ΔP_{tie1} **e** ΔP_{tie2} **f** ΔP_{tie3}

2015) and modified GWO (MGWO) (Padhy et al. 2017), the system is first considered to be driven through distinct integral controllers only. The gains of these controllers are then optimized employing DSA and J_{ITAE} by considering a 1% SLP. DSA tuned controller parameters and the respective numerical results of multi-source single-area EPS with integral controllers are delineated in Table 5. The corresponding solutions pertaining to the above cited studies are also provided in Table 5. It is easily noted from Table 5 that DSA outperforms the competitive approaches since less ITAE value is acquired by DSA ($J_{\text{ITAE}} = 0.4507$) compared to optimal controller ($J_{\text{ITAE}} = 0.9934$), DE ($J_{\text{ITAE}} = 0.5165$), TLBO ($J_{\text{ITAE}} = 0.5135$) and MGWO ($J_{\text{ITAE}} = 0.4514$), putting forward that the tuning performance of DSA is better than the rest. The best algorithm after DSA is MGWO, which found more or less the same result as DSA. As a result,

minimum settling time of frequency deviation is got with DSA and MGWO compared to other optimizers.

The resulting frequency deviation response following a 1% SLP for the same EPS and identical controller is shown in Fig. 10. It is found that the settling time of DSA- and MGWO-based responses is shorter than others as highlighted by the marks "●". The zoom views of the deviations in Fig. 10b also show that DSA tuned integral controller is able to provide smaller peak overshoot than its closest competitor, MGWO optimized integral controller. This improvement observed in the response can be attributed to the less value of J_{ITAE} achieved by DSA.

To improve the dynamic behavior of test system-4, integral controller is replaced by the designed FOPI–FOPD cascade controller. DSA optimized controller parameters and the respective system results with FOPI–FOPD cascade controller are given and compared in Table 6 with that of DSA tuned FOPID controller and other available results based on recently proposed MGWO tuned PI, PID and cascade PIPD controllers (Padhy et al. 2017). The results in Table 6 showcase easily the excellence of DSA

Table 5 Optimized integral controller parameters and T_s/J_{ITAE} results of test system-4

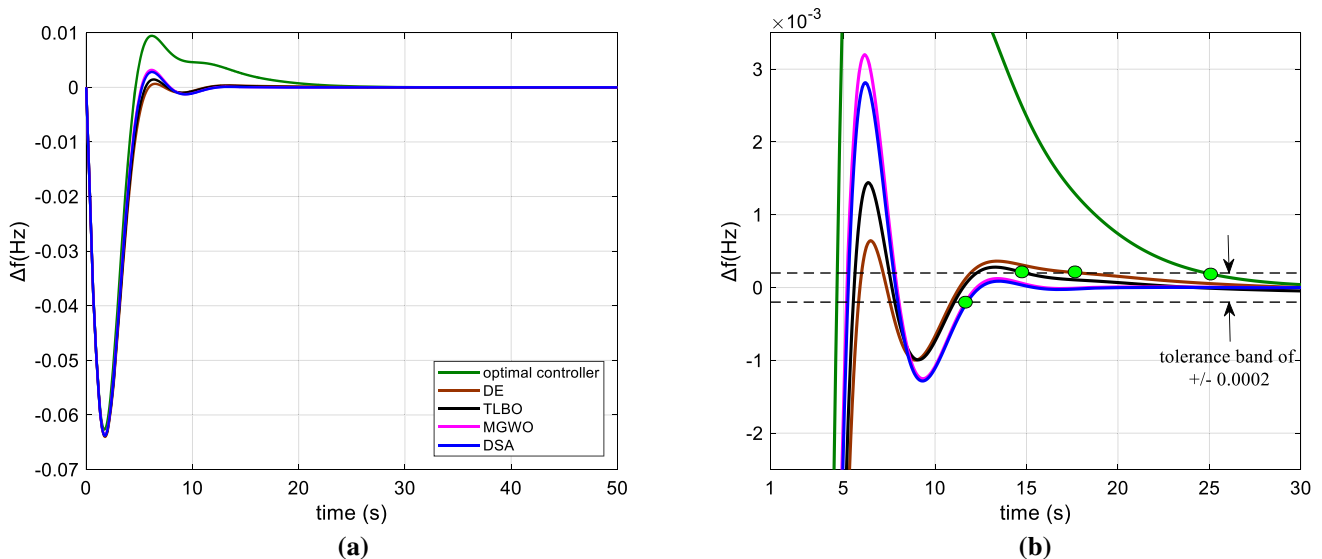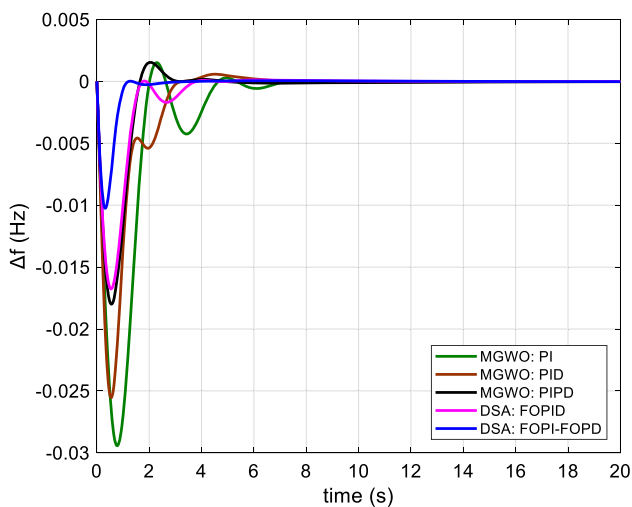| Algorithm	Optimal controller (Parmar et al. 2012)	DE (Mohanty et al. 2014)	TLBO (Barisal 2015)	MGWO (Padhy et al. 2017)	DSA
Controller parameters	$K_{i1} = 0.1514$	$K_{i1} = 0.0516$	$K_{i1} = 0.0511$	$K_{i1} = 0.0423$	$K_{i1} = 0.0416$
	$K_{i2} = 0.0131$	$K_{i2} = 0.0071$	$K_{i2} = 0.0041$	$K_{i2} = 0.0141$	$K_{i2} = 0.0144$
	$K_{i3} = 0.0708$	$K_{i3} = 0.1701$	$K_{i3} = 0.1847$	$K_{i3} = 0.2191$	$K_{i3} = 0.2149$
T_s (s) (2% band)					
Δf	24.82	17.91	14.91	11.75	11.75
J_{ITAE}	0.9934	0.5165	0.5135	0.4514	0.4507

Fig. 10 Comparison of frequency deviation responses after a 1% SLP for test system-4 using integral controllers tuned by different approaches

Table 6 Optimized controller parameters and T_s/J_{ITAE} results of test system-4

Algorithm	MGWO: PI (Padhy et al. 2017)	MGWO: PID (Padhy et al. 2017)	MGWO: PIPD (Padhy et al. 2017)	DSA: FOPID	DSA: FOPI-FOPD
Controller parameters	**Unit 1: Thermal**	**Unit 1: Thermal**	**Unit 1: Thermal**	**Unit 1: Thermal**	**Unit 1: Thermal**
	$K_p = 1.9995$	$K_p = 1.9995$	$K_{p1} = -0.2828$	$K_p = 1.9999$	$K_{p1} = -2$
	$K_i = 0.2391$	$K_i = 0.1637$	$K_{p2} = 0.0084$	$K_i = 2.0000$	$K_{p2} = -2$
	Unit 2: Hydro	$K_d = 0.4633$	$K_i = -1.7898$	$K_d = 0.5826$	$K_i = -2$
	$K_p = 0.0189$	**Unit 2: Hydro**	$K_d = -1.9978$	$\lambda = 0.4049$	$K_d = -2$
	$K_i = 0.0048$	$K_p = 0.4779$	**Unit 2: Hydro**	$\mu = 1.2184$	$\lambda = 0.8883$
	Unit 3: Gas	$K_i = 0.0906$	$K_{p1} = 0.1610$	**Unit 2: Hydro**	$\mu = 0.5116$
	$K_p = 0.0507$	$K_d = 0.9258$	$K_{p2} = -0.6917$	$K_p = -1.2615$	**Unit 2: Hydro**
	$K_i = 0.9633$	**Unit 3: Gas**	$K_i = -0.5022$	$K_i = 0.3340$	$K_{p1} = -1.2377$
		$K_p = 0.1918$	$K_d = -0.4581$	$K_d = 0.6897$	$K_{p2} = 1.3189$
		$K_i = 1.9995$	**Unit 3: Gas**	$\lambda = 0.98890$	$K_i = 0.3657$
		$K_d = 0.1192$	$K_{p1} = 0.0115$	$\mu = 0.4366$	$K_d = 0.6020$
			$K_{p2} = -1.9978$	**Unit 3: Gas**	$\lambda = 0.6953$
			$K_i = -1.9978$	$K_p = 2.0000$	$\mu = 0.8743$
			$K_d = -0.1134$	$K_i = 1.9899$	**Unit 3: Gas**
				$K_d = 0.0407$	$K_{p1} = -2$
				$\lambda = 1.1440$	$K_{p2} = -1.3423$
				$\mu = 0.8043$	$K_i = 2$
					$K_d = 1.2254$
					$\lambda = 0.7158$
					$\mu = 0.5336$
T_s (s) (2% band)					
Δf	6.85	6.10	2.83	3.58	2.24
J_{ITAE}	0.0572	0.0375	0.0292	0.0187	0.0070

Fig. 11 Comparison of frequency deviation responses after a 1% SLP for test system-4

tuned FOPI–FOPD cascade controller in minimizing J_{ITAE} value to 0.0070 from MGWO tuned PI ($J_{ITAE} = 0.0572$), PID ($J_{ITAE} = 0.0375$), cascade PIPD ($J_{ITAE} = 0.0292$) and DSA tuned FOPID ($J_{ITAE} = 0.0187$) controllers. Hence, improved settling time of Δf response is achieved by our proposal in comparison with other alternatives.

To investigate the time-domain simulation results, a 1% SLP is applied to the system at the instant $t = 0$ and system frequency deviations with different optimized controllers are depicted in Fig. 11. Recalling from the previous analysis that the search performance of DSA and MGWO is similar, then it may be noted that the designed FOPI–FOPD cascade controller performs amazingly better than other indicated controllers in substantially boosting the system dynamic response.

b. Two-area multi-source power system

Table 7 Optimized controller parameters and T_s/J_{ITAE} results of test system-5

Algorithm	DE: PID (Mohanty et al. 2014)	MGWO: PID (Padhy et al. 2017)	hSFS-PS: PID (Padhy and Panda 2017)	DSA: FOPID	DSA: FOPI-FOPD
Controller parameters	**Unit 1: Thermal**	**Unit 1: Thermal**	**Unit 1: Thermal**	**Unit 1: Thermal**	**Unit 1: Thermal**
	$K_p = 0.7790$	$K_p = 1.7502$	$K_p = -1.7074$	$K_p = 1.9998$	$K_{p1} = -2$
	$K_i = 0.2762$	$K_i = -0.0087$	$K_i = -1.9589$	$K_i = 2.0000$	$K_{p2} = -2$
	$K_d = 0.6894$	$K_d = 0.7499$	$K_d = -1.3934$	$K_d = 1.9999$	$K_i = -2$
	Unit 2: Hydro	**Unit 2: Hydro**	**Unit 2: Hydro**	$\lambda = 0.5021$	$K_d = -2$
	$K_p = 0.5805$	$K_p = 0.3110$	$K_p = -0.7453$	$\mu = 0.2386$	$\lambda = 0.5040$
	$K_i = 0.2291$	$K_i = 0.3102$	$K_i = 0.1375$	**Unit 2: Hydro**	$\mu = 0.0100$
	$K_d = 0.7079$	$K_d = 0.0034$	$K_d = -0.9896$	$K_p = 1.2029$	**Unit 2: Hydro**
	Unit 3: Gas	**Unit 3: Gas**	**Unit 3: Gas**	$K_i = 1.1908$	$K_{p1} = 1.7433$
	$K_p = 0.5023$	$K_p = 0.0091$	$K_p = -1.8253$	$K_d = -0.4375$	$K_{p2} = -2$
	$K_i = 0.9529$	$K_i = 1.2409$	$K_i = -1.6813$	$\lambda = 0.5072$	$K_i = -2$
	$K_d = 0.6569$	$K_d = 0.6901$	$K_d = -0.1628$	$\mu = 0.3748$	$K_d = -1.3626$
				Unit 3: Gas	$\lambda = 0.9506$
				$K_p = 0.9272$	$\mu = 0.0877$
				$K_i = 2.0000$	**Unit 3: Gas**
				$K_d = 1.9999$	$K_{p1} = -2$
				$\lambda = 1.2105$	$K_{p2} = -1.7815$
				$\mu = 1.2682$	$K_i = -2$
					$K_d = -2$
					$\lambda = 0.8692$
					$\mu = 1.2000$
T_s (s) (2% band)					
Δf_1	20.91	15.69	11.47	8.31	1.81
Δf_2	20.80	20.05	13.66	6.25	4.51
ΔP_{tie}	11.54	17.82	12.28	6.51	3.98
J_{ITAE}	1.0566	0.9197	0.3818	0.1557	0.0461

Our last analysis for corroborating the performance of proposed DSA tuned FOPI–FOPD cascade controller is toward a more realistic EPS model where a total of six generating units are cooperating to supply a given load under different circumstances. The transfer function model of this system is shown in Fig. 4 and the nominal system parameters are provided in "Appendix A.5" section. In this case, the controller parameters are optimized for a 2% SLP enforced in area-1. The optimized controller parameters along with some system results using the designed controller are reported in Table 7. Moreover, comparisons with other approaches such as DE (Mohanty et al. 2014), MGWO (Padhy et al. 2017) and hSFS-PS (Padhy and Panda 2017) optimized PID controllers as well as DSA optimized FOPID controller are also presented. Table 7 divulges that less J_{ITAE} value is achieved with DSA tuned FOPID controller ($J_{ITAE} = 0.1557$) in comparison with DE ($J_{ITAE} = 1.0566$), MGWO ($J_{ITAE} = 0.9197$) and hSFS-PS ($J_{ITAE} = 0.3818$) tuned PID controllers. However, the value of J_{ITAE} offered by the proposed DSA tuned FOPI–

FOPD cascade controller is minimum ($J_{ITAE} = 0.0461$), resulting in smaller settling times of Δf_1, Δf_2 and ΔP_{tie} responses. As a result, enriched system performance is gained with DSA tuned FOPI–FOPD cascade controller over all other competing approaches.

Comparative dynamic responses of the two-area multi-source EPS for a 2% SLP occurring in area-1 at $t = 0$ are shown in Fig. 12. Following the critical observation of Fig. 12, it is recognized that the system performance offered by the proposed approach is more prolific in every respect of settling time/undershoot/overshoot than that of DSA tuned FOPID controller and the others prevalent in the literature.

6 Conclusions

FOPI–FOPD cascade controller is originally introduced in this paper as an effective remedy for LFC problem of diverse single-/multi-area single-/multi-unit EPSs. To
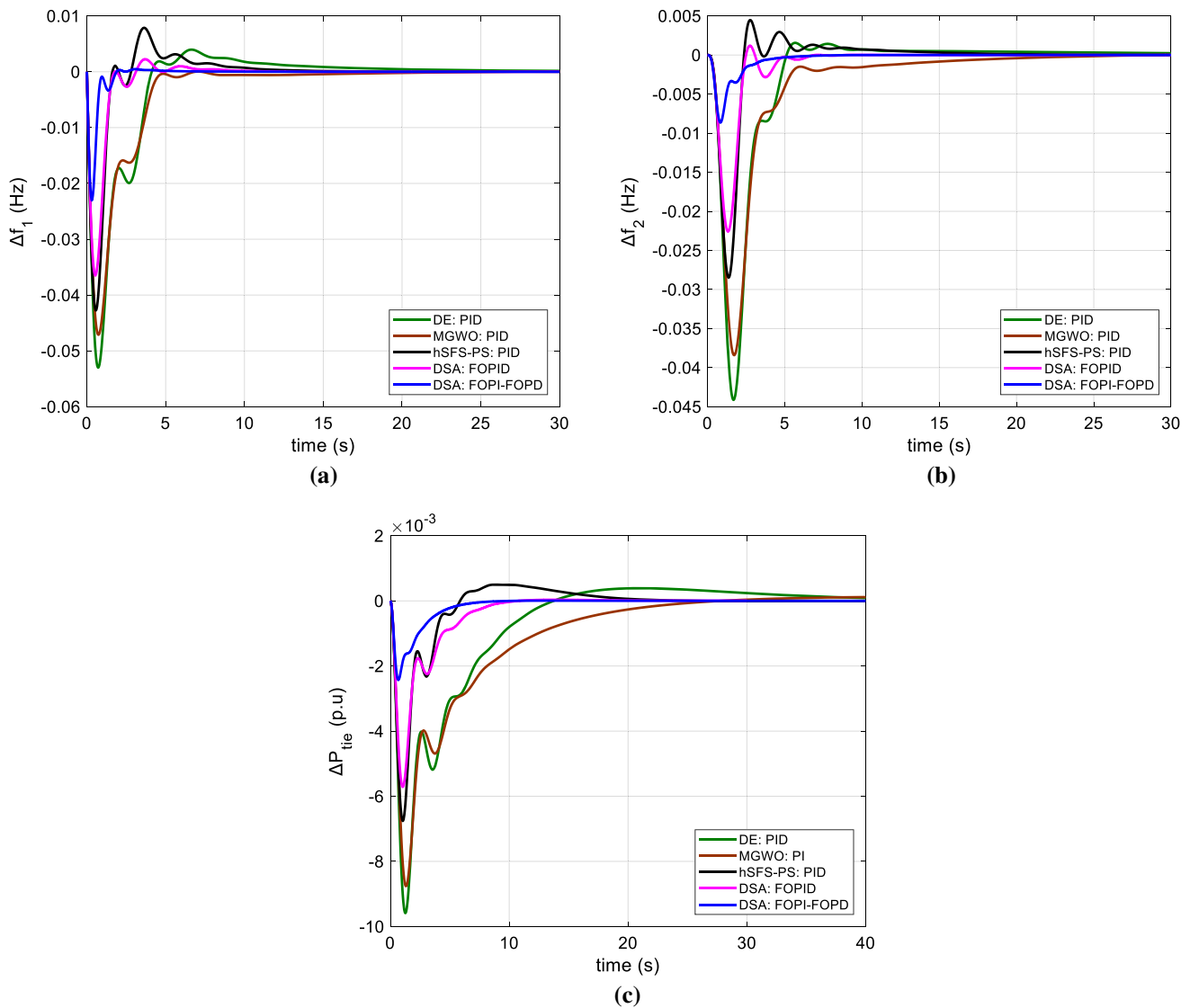
Fig. 12 Comparison of time-domain responses for test system-5 after a 2% SLP in area-1 **a** Δf_1 **b** Δf_2 **c** ΔP_{tie}

avoid improper gain scheduling, DSA, as the recently proposed powerful optimizer, is adopted to tune the designed controller parameters using J_{ITAE}. In each of the test cases including linear two-area non-reheat thermal EPS, nonlinear two-area non-reheat thermal EPS with GDB nonlinearity, three-area hydrothermal EPS considering GRC effect, multi-source single-area EPS and two-area multi-source EPS, the performance of the proposed approach is checked by contrasting its responses with that of DSA tuned FOPID controller and also well-recognized contributions recently appeared in the field. The results carefully collected have proved the higher credit of DSA tuned FOPI–FOPD cascade controller compared to DSA tuned FOPID and other existing solutions in terms of minimum value of J_{ITAE} and improved settling time/

undershoot/overshoot of deviation in area frequency and tie-line power responses. On the other hand, DSA is found to be effective and robust in searching for optimal controller parameters and it is authenticated that the designed DSA tuned FOPI-FOPD cascade controller can be thought of as a prolific solution, contributing notably to LFC performances of several EPSs.

For future works, a number of search directions can be advised for possible further improvements. In lieu of DSA, other latest metaheuristics may be tried out to optimize the proposed controller gains. High voltage direct current (HVDC) link and plug in electric vehicles (PEV) could be also included in the studied models as an axillary service in addition and parallel with existing AC tie-line. Moreover, modifying the existent controllers

with taking benefits of fractional calculus would be worthy to investigate.

Compliance with ethical standards

Conflict of interest The author does not have any conflict of interest.

Appendix A

A.1 Nominal parameters of test system-1 are (Ali and Abd-Elazim 2011; Panda et al. 2013; Sahu et al. 2015, 2016)

$f = 60$ Hz, $B = 0.425$ p.u MW/Hz, $R = 2.4$ Hz/pu, $T_g = 0.03$ s, $T_t = 0.3$ s, $K_{ps} = 120$ Hz/pu, $T_{ps} = 20$ s, $T_{12} = 0.545$ p.u MW/rad.

A.2 Nominal parameters of test system-2 are (Panda et al. 2013; Sahu et al. 2016; Çelik 2020; Gozde and Taplamacioglu 2011)

$f = 60$ Hz, $B = 0.425$ p.u MW/Hz, $R = 2.4$ Hz/pu, $T_g = 0.2$ s, $T_t = 0.3$ s, $K_{ps} = 120$ Hz/pu, $T_{ps} = 20$ s, $T_{12} = 0.444$ p.u MW/rad.

A.3 Nominal parameters of test system-3 are (Panda et al. 2013; Çelik 2020; Nanda et al. 2006)

$f = 60$ Hz, $B = 0.425$ p.u MW/Hz, $R = 2.4$ Hz/pu, $T_g = 0.08$ s, $K_r = 0.5$, $T_r = 10$ s, $T_t = 0.3$ s, $K_p = 1.0$, $K_d = 4.0$, $K_i = 5.0$, $T_w = 1$ s, $K_{ps} = 120$ Hz/pu, $T_{ps} = 20$ s, $T_{12} = T_{23} = T_{13} = 0.086$ p.u MW/rad.

A.4 Nominal parameters of test system-4 are (Mohanty et al. 2014; Padhy et al. 2017; Parmar et al. 2012; Barisal 2015)

$f = 60$ Hz, $R = 2.4$ Hz/pu, $T_{sg} = 0.08$ s, $K_r = 0.3$, $T_r = 10$ s, $T_t = 0.3$ s, $T_{gh} = 0.2$ s, $T_{rs} = 5$ s, $T_{rh} = 28.75$ s $T_w = 1$ s, $b_g = 0.05$ s, $c_g = 1$, $X_c = 0.6$ s, $Y_c = 1$ s, $T_{cr} = 0.01$ s, $T_f = 0.23$ s, $T_{cd} = 0.2$ s, $K_T = 0.543478$ pu, $K_H = 0.326084$ pu, $K_G = 0.130438$ pu, $K_{ps} = 68.9566$ Hz/pu MW, $T_{ps} = 11.49$ s

A.5 Nominal parameters of test system-5 are (Mohanty et al. 2014; Padhy et al. 2017; Padhy and Panda 2017)

$f = 60$ Hz, $B = 0.4312$ pu, $R = 2.4$ Hz/pu, $T_{sg} = 0.08$ s, $K_r = 0.3$, $T_r = 10$ s, $T_t = 0.3$ s, $T_{gh} = 0.2$ s, $T_{rs} = 5$ s,

$T_{rh} = 28.75$ s $T_w = 1$ s, $b_g = 0.05$ s, $c_g = 1$, $X_c = 0.6$ s, $Y_c = 1$ s, $T_{cr} = 0.01$ s, $T_f = 0.23$ s, $T_{cd} = 0.2$ s, $K_T = 0.543478$ pu, $K_H = 0.326084$ pu, $K_G = 0.130438$ pu, $T_{12} = 0.0433$, $K_{ps} = 68.9566$ Hz/pu MW, $T_{ps} = 11.49$ s

References

Ali ES, Abd-Elazim SM (2011) Bacteria foraging optimization algorithm based load frequency controller for interconnected power system. Int J Electr Power Energy Syst 33(3):633–638

Arya Y (2019a) Impact of ultra-capacitor on automatic generation control of electric energy systems using an optimal FFOID controller. Int J Energy Res 43:8765–8778

Arya Y (2019b) A novel CFFOPI-FOPID controller for AGC performance enhancement of single and multi-area electric power systems. ISA Trans. https://doi.org/10.1016/j.isatra.2019.11.025

Arya Y (2019c) A new optimized fuzzy FOPI–FOPD controller for automatic generation control of electric power systems. J Frankl Inst 356(11):5611–5629

Arya Y (2019d) AGC of restructured multi-area multi-source hydrothermal power systems incorporating energy storage units via optimal fractional-order fuzzy PID controller. Neural Comput Appl 31(3):851–872

Arya Y, Kumar N (2017a) Design and analysis of BFOA-optimized fuzzy PI/PID controller for AGC of multi-area traditional/ restructured electrical power systems. Soft Comput 21:6435–6452

Arya Y, Kumar N (2017b) BFOA-scaled fractional order fuzzy PID controller applied to AGC of multi-area multi-source electric power generating systems. Swarm Evolut Comput 32:202–218

Azarmi R, Tavakoli-Kakhki M, Sedigh AK, Fatehi A (2015) Analytical design of fractional order PID controllers based on the fractional set-point weighted structure: case study in twin rotor helicopter. Mechatronics 31:222–233

Barisal AK (2015) Comparative performance analysis of teaching learning based optimization for automatic load frequency control of multi-source power system. Int J Electr Power Energy Syst 66:67–77

Çelik E (2020) Improved stochastic fractal search algorithm and modified cost function for automatic generation control of interconnected electric power systems. Eng Appl Artif Intell 88:103407

Dahiya P, Sharma V, Naresh R (2015) Solution approach to automatic generation control problem using hybridized gravitational search algorithm optimized PID and FOPID controllers. Adv Electr Comput Eng 15(2):23–34

Dash P, Saikia LC, Sinha N (2014) Comparison of performances of several Cuckoo search algorithm based 2DOF controllers in AGC of multi-area thermal system. Int J Electr Power Energy Syst 55:429–436

Dash P, Saikia LC, Sinha N (2016) Flower pollination algorithm optimized PI–PD cascade controller in automatic generation control of a multi-area power system. Electr Power Energy Syst 82:19–28

Gozde H, Taplamacioglu MC (2011) Automatic generation control application with craziness based particle swarm optimization in a thermal power system. Int J Electr Power Energy Syst 33(1):8–16

Gozde H, Taplamacioglu MC, Kocaarslan İ (2012) Comparative performance analysis of artificial bee colony algorithm in

automatic generation control for interconnected reheat thermal power system. Int J Electr Power Energy Syst 42(1):167–178

Guha D, Roy PK, Banerjee S (2016a) Load frequency control of large scale power system using quasi-oppositional grey wolf optimization algorithm. Int J Eng Sci Technol 19(4):1693–1713

Guha D, Roy PK, Banerjee S (2016b) Load frequency control of interconnected power system using grey wolf optimization. Swarm Evolut Comput 27:97–115

Guha D, Roy P, Banerjee S (2017a) Quasi-oppositional symbiotic organism search algorithm applied to load frequency control. Swarm Evolut Comput 33:46–67

Guha D, Roy PK, Banerjee S (2017b) Study of differential search algorithm based automatic generation control of an interconnected thermal-thermal system with governor dead-band. Appl Soft Comput 52:160–175

Guha D, Roy PK, Banerjee S (2018) Application of backtracking search algorithm in load frequency control of multi-area interconnected power system. Ain Shams Eng J 9:257–276

Hota PK, Mohanty B (2016) Automatic generation control of multi source power generation under deregulated environment. Int J Electr Power Energy Syst 75:205–214

Ismayil C, Sreerama KR, Sindhu TK (2014) Automatic generation control of single area thermal power system with fractional order PID ($PI^\lambda D^\mu$) controllers. In: Proceedings of the 3rd international conference on advances in control and optimization of dynamical systems, March 13–15, Kanpur, India, pp 552–557

Jesus IS, Machado JAT, Barbosa RS (2010) Control of a heat diffusion system through a fractional order nonlinear algorithm. Comput Math Appl 59(5):1687–1694

Jezierski E, Ostalczyk P (2009) Fractional-order mathematical model of pneumatic muscle drive for robotic applications. Robot Motion Control LNCIS 396:113–122

Khuntia SR, Panda S (2012) Simulation study for automatic generation control of a multi-area power system by ANFIS approach. Appl Soft Comput 12:333–341

Kumar N, Tyagi B, Kumar V (2016) Deregulated multi area AGC scheme using BBBC-FOPID controller. Arab J Sci Eng 42(7):2641–2649

Mandal B, Roy PK (2014) Multi-objective optimal power flow using quasi-oppositional teaching learning based optimization. Appl Soft Comput 21:590–606

Mohanty B, Panda S, Hota PK (2014a) Controller parameters tuning of differential evolution algorithm and its application to load frequency control of multi-source power system. Int J Electr Power Energy Syst 54:77–85

Mohanty B, Panda S, Hota PK (2014b) Differential evolution algorithm based automatic generation control for interconnected power systems with non-linearity. Alex Eng J 53:537–552

Mousavi Y, Alfi A (2015) A memetic algorithm applied to trajectory control by tuning of fractional order proportional-integral derivative controllers. Appl Soft Comput 36:599–617

Naderi E, Pourakbari-Kasmaei M, Abdi H (2019) An efficient particle swarm optimization algorithm to solve optimal power flow problem integrated with FACTS devices. Appl Soft Comput 80:243–262

Nanda J, Parida M, Kalam A (2006) Automatic generation control of a multi-area power system with conventional integral controllers. In: Proceedings AUPEC 2006, Melbourne, Australia

Nayak JR, Shaw B, Sahu BK (2018) Application of adaptive-SOS (ASOS) algorithm based interval type-2 fuzzy-PID controller with derivative filter for automatic generation control of an interconnected power system. Int J Eng Sci Technol 21(3):465–485

Nithilasaravanan K, Thakwani N, Mishra P, Kumar V, Rana KPS (2019) Efficient control of integrated power system using self-tuned fractional-order fuzzy PID controller. Neural Comput Appl 31:4137–4155

Nour EL, Kouba Y, Menaa M, Hasni M, Boudour M (2018) A novel optimal combined fuzzy PID controller employing dragonfly algorithm for solving automatic generation control problem. Electr Power Compon Syst 46(19–20):2054–2070

Oustaloup A, Levron F, Matthieu B, Nanot FM (2000) Frequency-band complex noninteger differentiator: characterization and synthesis. IEEE Trans Circuits Syst I Fundam Theory Appl 47(1):25–39

Padhy S, Panda S (2017) A hybrid stochastic fractal search and pattern search technique based cascade PI–PD controller for automatic generation control of multi-source power systems in presence of plug in electric vehicles. CAAI Trans Intell Technol 2:12–25

Padhy S, Panda S, Mahapatra S (2017) A modified GWO technique based cascade PI–PD controller for AGC of power systems in presence of plug in electric vehicles. Int J Eng Sci Technol 20(2):427–442

Pan I, Das S (2015) Fractional order load-frequency control of interconnected power systems using chaotic multi-objective optimization. Appl Soft Comput 29:328–344

Panda S, Mohanty B, Hota PK (2013) Hybrid BFOA-PSO algorithm for automatic generation control of linear and nonlinear interconnected power systems. Appl Soft Comput 13:4718–4730

Parmar KPS, Majhi S, Kothari DP (2012) Load frequency control of a realistic power system with multi-source power generation. Int J Electr Power Energy Syst 42:426–433

Patel NC, Debnath MK, Sahu BK, Das P (2019) 2DOF-PID controller-based load frequency control of linear/nonlinear unified power system. In: Bhaskar M, Dash S, Das S, Panigrahi B (eds) International conference on intelligent computing and applications. Advances in intelligent systems and computing, vol 846. Springer, Singapore

Podlubny I (1999) Fractional-order systems and $PI^\lambda D^\mu$-controllers. IEEE Trans Autom Control 44(1):208–214

Rout UK, Sahu RK, Panda S (2013) Design and analysis of differential evolution algorithm based automatic generation control for interconnected power system. Ain Shams Eng J 4(3):409–421

Saha S (2010) Design of a fractional order phase shaper for iso-damped control of a PHWR under step-back condition. IEEE Trans Nucl Sci 57(3):1602–1612

Sahu RK, Panda S, Rou K (2013) DE optimized parallel 2-DOF PID controller for load frequency control of power system with governor dead-band nonlinearity. Int J Electr Power Energy Syst 49:19–33

Sahu RK, Panda S, Padhan S (2015a) A hybrid firefly algorithm and pattern search technique for automatic generation control of multi area power systems. Int J Electr Power Energy Syst 64:9–23

Sahu RK, Panda S, Sekhar GTC (2015b) A novel hybrid PSO-PS optimized fuzzy PI controller for AGC in multi area interconnected power systems. Int J Electr Power Energy Syst 64:880–893

Sahu RK, Panda S, Rout UK, Sahoo DK (2016a) Teaching learning based optimization algorithm for automatic generation control of power system using 2-DOF PID controller. Int J Electr Power Energy Syst 77:287–301

Sahu BK, Pati TK, Nayak JR, Panda S, Kar SK (2016b) A novel hybrid LUS-TLBO optimized fuzzy-PID controller for load frequency control of multi-source power system. Int J Electr Power Energy Syst 74:58–69

Saikia LC, Mishra S, Sinha N, Nanda J (2011) Automatic generation control of a multi area hydrothermal system using reinforced

learning neural network controller. Int J Electr Power Energy Syst 33(4):1101–1108

Sathya MR, Ansari MMT (2015) Load frequency control using Bat inspired algorithm based dual mode gain scheduling of PI controllers for interconnected power system. Int J Electr Power Energy Syst 64:365–374

Seyedali M (2016) Dragonfly algorithm: a new meta-heuristic optimization technique for solving single-objective, discrete, and multi-objective problems. Neural Comput Appl 27(4):1053–1073

Shiva CK, Shankar G, Mukherjee V (2015) Automatic generation control of power system using a novel quasi-oppositional harmony search algorithm. Int J Electr Power Energy Syst 73:787–804

Singh SP, Prakash T, Singh VP, Babu MG (2017) Analytic hierarchy process based automatic generation control of multi-area inter-connected power system using Jaya algorithm. Eng Appl Artif Intell 60:35–44

Sivalingam R, Chinnamuthu S, Dash SS (2017) A hybrid stochastic fractal search and local unimodal sampling based multistage PDF plus (1 + PI) controller for automatic generation control of power systems. J Frankl Inst 354:4762–4783

Sondhi S, Hote YV (2014) Fractional order PID controller for load frequency control. Energy Convers Manag 85:343–353

Venkatesh M, Sudheer G (2017) Optimal load frequency regulation of micro-grid using dragonfly algorithm. Int Res J Eng Technol 4(8):978–981

Vrdoljak K, Peric N, Petrovic I (2010) Sliding mode based load frequency controller in power systems. Electr Power Syst Res 80(5):514–527

Zamani A, Barakati SM, Yousofi-Darmian S (2016) Design of a fractional order PID controller using GBMO algorithm for load frequency control with governor saturation consideration. ISA Trans 64:56–66

Zeng GQ, Chen J, Dai YX, Li LM, Zheng CW, Chen MR (2015) Design of fractional order PID controller for automatic regulator voltage system based on multi-objective extremal optimization. Neurocomputing 160:173–184

Zhong J, Li L (2015) Tuning fractional-order $PI^{\lambda}D^{\mu}$ controllers for a solid-core magnetic bearing system. IEEE Trans Control Syst Technol 23(4):1648–1656